AD-A179 690 JOURNAL OF CHINESE SOCIETY OF ASTRONAUTICS (SELECTED ARTICLES)(U) FOREIGN TECHNOLOGY DIV WRIGHT-PATTERSON AFB OH X CHANG ET AL. 06 APR 87 FTD-ID(RS)T-0432-86 1/1

UNCLASSIFIED F/G 21/8.2 NL

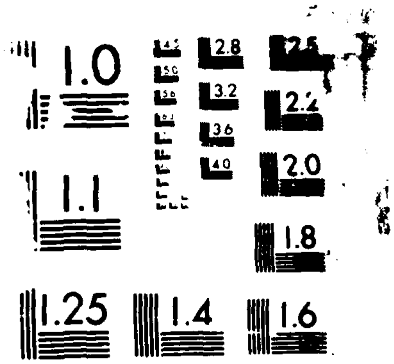

Mi

AD-A179 690

FTD-ID(RS)T-0432-86

FOREIGN TECHNOLOGY DIVISION

AIR FORCE SYSTEMS COMMAND

JOURNAL OF CHINESE SOCIETY OF ASTRONAUTICS

(Selected Articles)

FOREIGN TECHNOLOGY DIVISION

Approved for public release;
Distribution unlimited.

FTD-ID(RS)T-0432-86

Edited

~~HUMAN TRANSLATION~~

FTD-ID(RS)T-0432-86 6 April 1987

MICROFICHE NR: FTD-87-C-000276

JOURNAL OF CHINESE SOCIETY OF ASTRONAUTICS
(Selected Articles)

English pages: 82

Source: Yuhang Xuebao, Nr. 1, January 1985, pp. 11-23;
47-58; 59-77

Country of origin: China
Translated by: SCITRAN
F33657-84-D-0165
Requester: FTD/TQTA
Approved for public release; Distribution unlimited.

THIS TRANSLATION IS A RENDITION OF THE ORIGINAL FOREIGN TEXT WITHOUT ANY ANALYTICAL OR EDITORIAL COMMENT. STATEMENTS OR THEORIES ADVOCATED OR IMPLIED ARE THOSE OF THE SOURCE AND DO NOT NECESSARILY REFLECT THE POSITION OR OPINION OF THE FOREIGN TECHNOLOGY DIVISION.	PREPARED BY: TRANSLATION DIVISION FOREIGN TECHNOLOGY DIVISION WPAFB, OHIO.

TABLE OF CONTENTS

GRAPHICS DISCLAIMER

All figures, graphics, tables, equations, etc. merged into this translation were extracted from the best quality copy available.

DISCLAIMER NOTICE

ONE-DIMENSIONAL TWO-PHASE FLOW IN COMBUSTION CHAMBER OF SOLID PROPELLANT ROCKET MOTORS

CHANG XIANQI

ABSTRACT

In this paper, a numerical solution of basic equation for /23
one dimensional two-phase nonequilibrium flow in a combustion chamber of solid propellant rocket motors is discussed in detail, the effect of particle size on flow field in combustion chamber and pressure-time curves is analyzed, and some useful conclusions are obtained in comparison with results of one dimensional two-phase constant lag flow in combustion chamber. It is useful for predicting pressure-time curves accurately and providing accurate boundary conditions for the calculation of two-phase flow through the nozzle.

Nomenclature

A - duct cross section area

A_b - Burning area of charge

A_Q - Thermal equivalent of work

A_t - Area of the nozzle throat

$\overline{M}$ - Mean molecular weight of gas

n - Pressure exponent

P - Pressure

P_s - Total pressure

b - Burning speed coefficient

C* - Characteristic speed of propellant

C_l - Particulate specific heat

C_{pg} - Specific heat of gaseous phase at constant pressure

g - Gravitational acceleration

h - Enthalpy per unit mass

H_s - Total enthalpy in 1 kg of two-phase mixture

H_{sg} - Total enthalpy in 1 kg of gas

H_{sp} - Total enthalpy in 1 kg of liquid

κ - Ratio of specific heat of gas

K - Particle velocity lag coefficient

K_1 - Surface - throat ratio $\quad K_1 = \frac{A_b}{A_t}$

l - Charge length

L - Particle temperature lag coefficient

$\dot{m}$ - Mass flow rate of two-phase mixture

$\dot{m}_g$ - Mass flow rate of gas

q - Heat flux of particles per unit mass

r - Burning rate

r_p - Radius of particles

R_g - Gas constant of gaseous phase

S - Duct circumference

t - Time

T - Temperature

T_o - Total temperature of charge head gaseous phase

T_s - Total temperature of gaseous phase

v - Velocity /12

x - Axial coordinate

X - Particle resistance per unit mass

Y_C - Outer radius of charge

ρ - Density

ρ_t - Density of propellant

$\dot{m}_p$ - Mass flow rate of condensed phase

M_g - Mach number of gaseous phase

ρ_{mp} - Density of Al_2O_3 material

ε - Fraction of particle mass flow rate, $\varepsilon = \frac{\dot{m}_p}{\dot{m}}$

λ_g - Coefficient of thermal conductivity of gaseous phase

μ_g - Coefficient of dynamic viscosity of gaseous phase

SUBSCRIPTS

g - Gas phase

o - Cross section of charge head

t - Cross section of nozzle throat

P - Condensed phase

L - Cross section at the charge tip

i - initial value

1. PREFACE

Modern composite solid propellants are mixed with a certain amount of aluminum powder for increasing energy and decreasing unsteady burning. When the aluminum mixed propellant burns, Al_2O_3 particles are formed in liquid phase. The weight fraction can be up to 30-40%. Therefore, in combustion chambers and jet nozzles, the products of combustion actually are a mixture of gas and liquid.

There have been a lot of publications regarding two-phase flow in jet nozzles of a rocket motor. Most of them are devoted to one dimensional two-phase flow and two dimensional axial symmetrical two-phase flow in nozzles. There has been some progress. Two-phase flow in a combustion chamber is involved with mass, and has some new characteristics. The author has done research on one dimensional two-phase constant lag flow in a combustion chamber [4], analyzing the particle velocity lag effects on the combustion chamber processes. This article studies the one dimensional two-phase nonequilibrium flow in a combustion chamber. Based upon the principle equations of one dimensional mass involving two-phase flow in a combustion chamber., it discusses the numerical solutions of the equations in detail, analyzes particle size effect on the chamber flow field and the pressure-time curve, and compares the results with that of constant lag flow. Some practical conclusions are reached. This gives precision in predicting pressure-time curve, and more accurate boundary conditions for calculation of two-phase flow in jet nozzles.

II. FUNDAMENTAL EQUATIONS

Assume:

1. Flow is one-dimensional and steady-state;
2. The friction and heat loss on the duct wall are negligible;
3. Al_2O_3 particles are spherical, uniform, and in the liquid phase; the particle volume and the Brownian motion effects on pressure are negligible;
4. The gas phase is an ideal gas at freezing point except in contact with particles and otherwise is inviscid;
5. No mass exchange between two phases;
6. The specific heat of gas and particles is constant /13

Based upon the above assumptions, the fundamental equations of two-phase flow in the combustion chamber are obtained as follows [1] and [3]:

Gas phase -

Mass Equation:

$$\frac{d}{dx}(\rho_g v_g A)=(1-\varepsilon)\rho_T r S \tag{1}$$

Momentum equation:

$$\frac{d}{dx}(\rho_g v_g^2 A)=-A\frac{dP}{dx}-X\rho_p A \tag{2}$$

Energy equation:

$$\frac{d}{dx}\left[\rho_g g v_g A\left(h_g+A_Q\frac{v_g^2}{2g}\right)\right]=(1-\varepsilon)\rho_T r S g H_{sg}-A_Q X\rho_p v_p A+q\rho_p A \tag{3}$$

in which $r=bP^n$

$h_g=C_{pg}T_g$

Condensed phase-

Mass Equation:

$$\frac{d}{dx}(\rho_p v_p A)=\varepsilon\rho_T r S \tag{4}$$

Momentum equation:

$$\frac{d}{dx}(\rho_p v_p^2 A) = X \rho_p A \tag{5}$$

Energy equation:

$$\frac{d}{dx}\left[\rho_p g v_p A\left(h_p + A_Q \frac{v_p^2}{2g}\right)\right] = \varepsilon \rho_T r S g H_{sp} + A_Q X \rho_p v_p A - q \rho_p A \tag{6}$$

Two-phase mixture-

Mass equation:

$$\frac{d\dot{m}}{dx} = \rho_T r S \tag{7}$$

Momentum equation:

$$\frac{d}{dx}(\rho_g v_g^2 A + \rho_p v_p^2 A) = -A \frac{dP}{dx} \tag{8}$$

Energy equation:

$$\frac{d}{dx}\left[\dot{m}_g\left(h_g + A_Q \frac{v_g^2}{2g}\right) + \dot{m}_p\left(h_p + A_Q \frac{v_p^2}{2g}\right)\right] = \rho_T r S H_s \tag{9}$$

in which

$$\dot{m}_g = \rho_g v_g A$$
$$\dot{m}_p = \rho_p v_p A$$
$$\dot{m} = \dot{m}_g + \dot{m}_p$$

III. SOME SUPPLEMENTARY RELATIONSHIPS

Equations (1)-(6) are not closed, therefore, we introduce the following supplementary relationships:

1. Gas-phase condition equation

   for an ideal gas -- $P = \rho_g g R_g T_g$ (10)

2. Condensed-phase condition equation.

When the Al_2O_3 particle temperature is greater than the melting point ($T_{pm}=2318°K$) assuming its specific heat is constant, then

$$h_p=h_{pm}+C_l(T_p-T_{pm}) \tag{11}$$

in which

C_l - Specific heat of liquid Al_2O_3 particle, 0.34327 KCal/kg. degree K; h_{pm} - Enthalpy of liquid Al_2O_3 at T_{pm}, 876.9498 KCal/kg

From (11) we have

$$dh_p=C_l dT_p \tag{12}$$

3. The particle resistance X[1,2] per unit mass

$$X=A_p(v_g-v_p) \tag{13}$$

Under the condition of combustion chambers, the particles carryout Stokes flow, at this moment

$$A_r=\frac{9}{2}\frac{\mu_g}{r_p^2\rho_{mp}}$$

in which $\mu_g=1.208\times10^{-8}T_g^{0.6}M^{0.5}$ (kg, sec/m^2)

4. The heat flux q [1,2] of particles per unit mass

$$q=B_p(T_p-T_g) \tag{14}$$

in which $B_p=\frac{3\lambda_g}{r_p^2\rho_{mp}}$

5. The total enthalpy H_s in 1 kg of two-phase mixture $H_s=(1-\varepsilon)H_{sg}+\varepsilon H_{sp}$.

From the assumption 2, H_s is constant along the channel, therefore, it is convenient to use the parameters ($v_g=v_p=0$, $T_g=T_p=T_0$) at the charge origin (x=0), to express H_s. Therefore

$$H_s=(1-\varepsilon)C_{pg}T_0+\varepsilon[h_{pm}+C_l(T_0-T_{pm})] \tag{15}$$

IV. COMPUTATIONAL EQUATIONS

Let

$$K \equiv \frac{v_p}{v_g} \qquad (0 \leqslant K \leqslant 1) \tag{16}$$

$$L \equiv \frac{T_0 - T_p}{T_0 - T_g} \qquad (0 \leqslant L \leqslant 1) \tag{17}$$

Therefore particle velocity lag $= \frac{v_g - v_p}{v_g} = 1 - K$

particle temperature lag $= \frac{T_p - T_g}{T_0 - T_g} = 1 - L$

Here K,L are defined as particle velocity lag coefficient and temperature lag coefficient respectively.

Ignoring the effect of burning erosion, assuming the cross section area A of the charge duct is constant along the longitudinal axis, after an elaborate manipulation, the following numerical solution is obtained based upon the fundamental equations:

$$
\left.
\begin{aligned}
&\frac{dv_p}{dx} = A_p \frac{v_g - v_p}{v_p} - \frac{\varepsilon \rho_T r S}{\rho_p A} \\
&\frac{dv_g}{dx} = -\frac{R_g}{\rho_g (v_g^2 C_{pg} - g R_g T_g C_{pg} - A_Q R_g v_g^2)} \Big[g \rho_p h_g A_p \frac{v_g - v_p}{v_g} \\
&\qquad + \rho_p B_p (T_p - T_g) + A_Q \rho_p A_p (v_g - v_p)^2 + (1-\varepsilon) \rho_T r \frac{S}{A} g \\
&\qquad \cdot \left(H_{sg} + h_g + A_Q \frac{v_g^2}{2g} \right) \Big] - \frac{(1-\varepsilon) \rho_T r S}{\rho_g A} - \frac{\varepsilon}{1-\varepsilon} A_p \frac{v_g - v_p}{v_p} \\
&\frac{d\dot{m}}{dx} = \rho_T r S \\
&\rho_p = \frac{\varepsilon \dot{m}}{v_p A} \\
&\rho_g = \frac{(1-\varepsilon) \dot{m}}{v_g A} \\
&P = P_0 - (\rho_g v_g^2 + \rho_p v_p^2) \\
&T_g = \frac{P}{\rho_g g R_g} \\
&T_p = \frac{1}{\varepsilon C_l} \Big[\varepsilon C_l T_0 + (1-\varepsilon) C_{pg} T_0 - (1-\varepsilon) C_{pg} T_g \\
&\qquad - (1-\varepsilon) A_Q \frac{v_g^2}{2g} - \varepsilon A_Q \frac{v_p^2}{2g} \Big] \\
&M_g = \frac{v_g}{\sqrt{k g R_g T_g}} \\
&T_s = T_g \left(1 + \frac{k-1}{2} M_g^2 \right) \\
&P_s = P \left(1 + \frac{k-1}{2} M_g^2 \right)^{\frac{k}{k-1}}
\end{aligned}
\right\} \tag{18}
$$

in which $\qquad H_{sg}=C_{pg}T_s$

The system of equation (18) contains 3 ordinary differential equations and 8 algebraic equations, with the unknowns v_P、T_P、ρ_P, v_g、 T_g、 ρ_g、P、 P_s、T_s、M_g及$\dot{m}$, under the given boundary conditions, which can be solved by the Runge-Kutta numerical method.

V. INITIAL CONDITION AND BOUNDARY CONDITIONS

The initial condition of the equation:

When t=0, $S=S_i$, $A=A_{io}$. The value of A_i, S_i can be obtained by the actual shape of a charge duct, for a circular cross section of the duct.

$$S_i=2\pi y_i$$
$$A_i=\pi y_i^2$$

y_i is the duct initial radius.

The boundary conditions of equations:

If the charge fills the annular space between two closed end coaxial cylinders, the boundary conditions are (refer to Figure 1); at the charge head (x=0) cross section

$$\begin{aligned}
&v_{P0}=v_{g0}=0\\
&\dot{m}_0=0\\
&T_{g0}=T_{P0}=T\\
&P=P_0\\
&\rho_{g0}=\frac{P_0}{gR_gT_0}\\
&\rho_{P0}=\frac{\varepsilon}{1-\varepsilon}\,\frac{v_{g0}}{v_{P0}}\rho_{g0}=\frac{\varepsilon}{1-\varepsilon}\,\frac{\rho_{g0}}{K_0}
\end{aligned} \qquad (19)$$

in which, the total temperature of the charge head gaseous phase T_0 is equal to the burning temperature of the charge. P_0 is the corresponding pressure. Before solving the equation, it is unknown. Therefore, its value has to be determined by the iteration process in the numerical solution. The particle density ρ_{p0} at the charge head is $\frac{0}{0}$ an uncertain value. To determine this value, the value of K_0 has to be obtained beforehand.

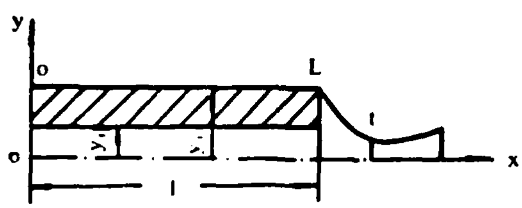

Figure 1.

At the charge end (x=l) cross section the mass flow rate $\dot{m}$ of the two-phase mixture passing through the cross section area at the charge end (x-l), should be equal to the mass flow rate $\dot{m}_t$ of the two-phase mixture passing through the throat of the jet nozzle, that is

$$\dot{m}_L = \dot{m}_t \tag{20}$$

$\dot{m}_L$ can be determined by the parameters of of the x=l cross section, that is

$$\dot{m}_L = A(\rho_{gL} v_{gL} + \rho_{pL} v_{pL}) \tag{21}$$

The present article is mainly about two-phase nonequilibrium flow in a combustion chamber. To avoid the numerical solution for one dimensional nonequilibrium two-phase flow in the jet nozzle, in the determination of the boundary condition of the charge end, it is assumed that the flow in the jet nozzle is a one dimensional two-phase constant lag flow, therefore:

$$\dot{m}_t = \frac{1}{1-\varepsilon} \frac{\bar{\Gamma}}{\sqrt{gR_gT_oC}} P_{sL} A_t \sqrt{\frac{k}{\bar{r}}} \tag{22}$$

in which

$$C = 1 + \frac{\varepsilon}{1-\varepsilon}\{K[k(1-K)+K] + (k-1)\delta LD\}$$

$$D = \frac{1 + \frac{\varepsilon}{1-\varepsilon}K^2}{1 + \frac{\varepsilon}{1-\varepsilon}\delta L}$$

$$\delta = \frac{C_l}{C_{Pg}}$$

$$\bar{r} = 1 + (k-1)\frac{D}{C}$$

$$\bar{\Gamma} = \sqrt{\bar{r}}\left(\frac{2}{\bar{r}+1}\right)^{\frac{\bar{r}+1}{2(\bar{r}-1)}}$$

where the value of K, L should be taken as the corresponding value at the end of the field length.

VI. THE DETERMINATION OF K_o, L_o

For obtaining the distribution of particle speed lag and temperature lag along the duct, and the numerical solution for a system of equations (18), the values of K, L at the charge head (x=0) have to be determined.

However, at x-0, both K and L are indeterminate forms, therefore, it is necessary to consider that at the charge head

$$K_0 = K_{x\to 0^+}$$
$$L_0 = L_{x\to 0^+}$$

1. The determination of K_0

   from l ' Hopital's rule

$$K_0 = \frac{v_p'|_{x\to 0^+}}{v_g'|_{x\to 0^+}} \qquad \text{(a)}$$

After transforming the first equation in the system of equations (18), we find that, at $x\to 0^+$, $v_p'|_{x\to 0^+}$ is also an indeterminate form of $\frac{0}{0}$. So

$$v_p'|_{x\to 0^+} = A_p \frac{v_g'|_{x\to 0^+} - v_p'|_{x\to 0^+}}{v_p'|_{x\to 0^+}} - v_p'|_{x\to 0^+}$$

For convenience, the subscript $x\to 0^+$ has been omitted in the following expression. After rearrangement it reads

$$\frac{2}{A_p} v_p'^2 + v_p' - v_g' = 0 \qquad \text{(b)}$$

With the help of the boundary condition (19), from the second equation in the system of equations (18) the following is derived that at $x\to 0^+$

$$v_g' = \frac{(1-\varepsilon)\rho_T r_0 S}{\rho_{g0} A} \qquad \text{(c)}$$

in which $r_0 = bP_0^n$

Substitute (c) into (b), it is obtained that at $x\to 0^+$

$$v_p' = \frac{-1 \pm \sqrt{1 + \frac{8}{A_p}\frac{(1-\varepsilon)\rho_T r_0 S}{\rho_{g0} A}}}{\frac{4}{A_p}} \qquad \text{(d)}$$

Because in a combustion chamber the flow involves an additional mass of particles, if the speed of a particle v_P increases, then $v'_P>0$, therefore, (d) should be positive which results in the sign in front of the square root being "+".

Substitute (d), (c) into (a), and set

$$a=\frac{4}{A_P}\ \frac{(1-\varepsilon)\rho_T r_0 S}{\rho_{g0} A} \tag{23}$$

then obtain

$$K_0=\frac{-1+\sqrt{1+2a}}{a} \tag{24}$$

2. The determination of L_o :

Same as above, from l' Hopital rule

$$L_0=\frac{T'_P|_{x\to 0^+}}{T'_g|_{x\to 0^+}} \tag{e}$$

It can be derived from the fundamental equations (1)-(6)

$$\frac{dT_P}{dx}=T'_P=\frac{1}{xC_l}\left(H_{SP}-h_P+A_Q\frac{v_P^2}{2g}\right)-\frac{B_P(T_P-T_g)}{v_P g C_l}$$

herein, $T'_P|_{x\to 0^+}$ is also an indeterminate form of $\frac{0}{0}$.

From l'Hopital rule it is obtained as

$$T'_P|_{x\to 0^+}=-T'_P|_{x\to 0^+}-\frac{B_P}{gC_l}\ \frac{T'_P|_{x\to 0^+}-T'_g|_{x\to 0^+}}{v'_P|_{x\to 0^+}}$$

Omitting the subscript $x\to 0^+$, then

$$2T'_P=-\frac{B_P}{gC_l}\ \frac{T'_P-T'_g}{v'_P} \tag{f}$$

let

$$\beta=\frac{B_P}{gC_l}\ \frac{1}{v'_P}$$

from equation (f) it is obtained

$$L_e = \frac{\beta}{2+\beta} \tag{25}$$

With the expressions of equations (d) and (23), the following is obtained:

$$\beta = \frac{4}{gC_l} \frac{B_p}{A_p} \frac{1}{(-1+\sqrt{1+2a})} \tag{26}$$

VII. NUMERICAL SOLUTION OF THE SYSTEM OF EQUATIONS

Under the boundary conditions (19), (20) and the initial condition, but use of the fourth order Runge-Kutta method the solution for the system of equations (18) can be obtained as follows:

1. At a fixed time t, the gas flow parameters $(v_g, T_g, \rho_g, P, P_s, T_s, M_g)$,. , the particle flow parameters (v_p, T_p, ρ_p) and the particle lag factor K, L distribution along the duct.

2. The pressure variation with respect to time in the combustion chamber.

In the boundary condition (19), the head pressure P_0 is unknown apriori, and has to be determined with the numerical solution process. The procedure is the following:

(1) Form $P_0^{(1)}=(C^*\rho_T bK_1)^{\frac{1}{1-n}}$ to compute the first approximate value;

(2) With the value of $P_o^{(1)}$ solve for the system of equations (18), and obtain the variation of parameters of the gas and the particle along the x-axis, then form equation (21), (22) and solve for $\dot{m}_L$ and $\dot{m}_t$;

(3) Let $\Delta\dot{m}=\dot{m}_t-\dot{m}_L$, and make a judgment on

$$\left|\frac{\Delta\dot{m}}{\dot{m}_t}\right|<\varepsilon_1 \qquad (27)$$

(ε_1 is a given allowable error, for instance $\varepsilon_1=0.01$) to see whether it is satisfied.

(4) If equation (27) is not true, and $\Delta\dot{m}>0$, take $P_0^{(2)}=P_0^{(1)}-\Delta P$ (ΔP is the given increase in pressure, for example $\Delta p=1$ kg/cm^2), otherwise take $P_0^{(2)}=P_0^{(1)}+\Delta P$, repeat the procedure for solving the system of equations (18), if the mass flow rate satisfies (27), then $P_o^{(2)}$ is the true value of the pressure at the charge head P_0;

(5) If the condition (27) still can not be satisfied, the following interpolation equation can be used for computing $P_o^{(n)}$:

$$P_0^{(n)}=P_0^{(n-1)}+\Delta\dot{m}^{(n-1)}\frac{P_0^{(n-1)}-P_0^{(n-2)}}{\Delta\dot{m}^{(n-2)}-\Delta\dot{m}^{(n-1)}} \qquad (n=3,4,5,\cdots\cdots)$$

then solve for the system of equations (18), till the mass flow rate satisfies equation (27). Figure 2 shows the flow chart of the numerical solution process, in which r_{cp} is the average burning speed along the length of the duct.

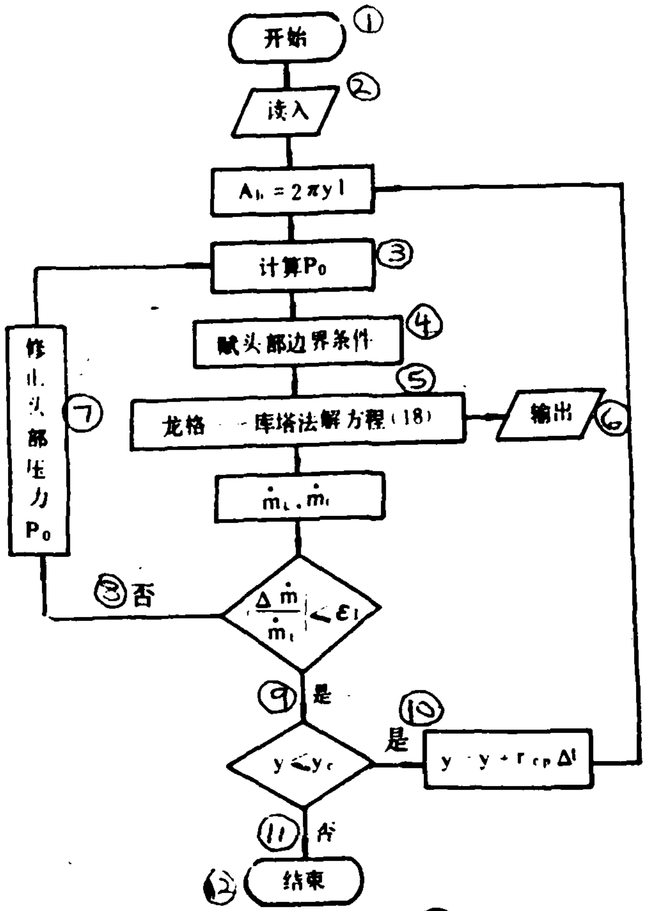

图2 计算框图

Figure 2.

Key: (1) start; (2) input; (3) compute P_0; (4) furnish boundary conditions; (5) Runge-Kutta method for solving the system of equations (18), (6) output, (7) adjust the head pressure P_0 (8) No, (9) Yes, (10) Yes, (11) No, (12) Stop, (13) Flow Chart of Computation.

VIII. THE EFFECT OF THE PARTICLE SIZE ON INTERNAL BALLISTIC PROPERTIES

As to a certain solid propellant rocket motor (ε=0.26), the pressure-time curve and the flow field in the combustion chamber have been computed for different sizes of particles.

Figure 3 shows the effect of the particle size on the Pressure-Time curve. It can be observed in the figure that the pressure in the combustion chamber decreases as the particle size increases. At t=0 sec., the variation of the combustion chamber pressure P_o with respect to the particle radius is shown in Figure 4. The decrease of the combustion chamber pressure will lead to a slowdown of the burning speed, increase the charge burning period and decrease the mass flow rate.

At t=0 sec., the variation of the gas parameters along the x-axis for the different particle sizes is shown in Figure 5. M_g solely increases with the distance, the rest of the parameters decrease with the distance. Because P_o decreases when the particle size increases, therefore P, P_s, ρ_g are affected by the particle size distinctively. The larger the particle size, the smaller are the values of them. But the particle size effect on T_g is negligible.

Figure 6 shows at t=0 sec. the distribution of the gas speed v_g and the particle speed v_p along the duct under different particle size conditions. Because the flow in the combustion chamber is involved with an increase in mass, both v_g and v_p increase along the length of the duct. But the particle size effect on v_g and v_p is different when particle size increases: v_g increases, but v_p decreases. This is because the particle of unit mass has a resistance to the gas of $\propto \frac{1}{r_p^2}$. When the particle size increases, X decreases, so the gas speed increases. At this moment the torque exerted on the particle by gas decreases. This results in the particle acceleration decreasing, therefore v_p becomes small. The density and temperature distribution of the particle are shown in Figure 7. It can be observed that ρ_p hardly decreases along the duct and T_p basically stays constant.

The effect of the particle size on the value of ρ_p is significant: when particle size increases, ρ_p increases too. But the effect on the value of T_p is negligible.

At t=0 sec., the particle speed lag factor K and temperature lag factor L distributions along the duct are shown in Figure 8. It can be observed that the value of K slightly decreases along the distance, but the value of L fundamentally stays constant. This indicates that in the combustion chamber, the particle speed lag (1-K) increases slightly along the length of the duct, but the temperature lag (1-L) basically stays constant. The smaller is the particle size, the smaller is the variation of K value along the distance. (Refer to Table 1.) Therefore when the particle size is small, the two-phase flow in the combustion chamber can be treated as the constant lag flow motion.

Table 1.

粒子半径 r_p (微米) (1)	K_e	装药末端 K 值降低 (%) (2)
2	0.9958	0.020
5	0.9752	0.082
10	0.9123	0.263
20	0.7538	0.478

Key: (1) The radius of the particle r_p (micrometer), (2) The decrease of K at the charge end

Table 2 lists, for different particle sizes, the comparison between the numerical solutions and constant lag flow computations of some important parameters in two-phase flow in a combustion chamber. Compared with the numerical solution, the combustion chamber pressure P_o and the total pressure at the end charge end obtained from the constant lag flow computation are comparatively low, and the rest of the parameters are comparatively high, but the deviation is less than 1%.

Table 2.

(2) r_p (微米)	P_0 (公斤/厘米²) (3)		P_{SL} (公斤/厘米²) (4)		V_{gL} (米/秒) (5)		V_{pL} (米/秒) (6)	
	数值解 (7)	常滞后 (8)	数值解 (9)	常滞后 (10)	数值解 (11)	常滞后 (12)	数值解 (13)	常滞后 (14)
5	18.66	18.57	18.42	18.38	119.64	120.46	116.58	117.44
10	18.42	18.37	18.20	18.18	120.90	121.50	110.00	110.82
20	17.92	17.87	17.70	17.68	123.82	124.26	92.74	93.62

Key: (2) Micrometer, (3) Kg/cm^2, (4) kg/cm^2, (5) m/sec, (6) m/sec, (7),(9),(11),(13) numerical solution, (8),(10),(12),(14) constant lag flow.

From equation (24),(25) it becomes known the values of K_o, L_o are functions of the particle radius r_p. Their variation with respect to r_p is shown in Figure 9. It can be seen in the Figure K_o, L_o values decrease when the particle size increases, which means, the particle speed lag and temperature lag increases as the particle size increases.

Besides, $K_o \leq L_o$, in the nonequilibrium flow in the combustion chamber, the lag of the particle speed is greater than the lag of the particle temperature.

IX. CONCLUSION

Through the above discussion the following conclusions are therefore obtained:

1. Because of the effect of the two-phase flow, the pressure of the combustion chamber decreases, and the larger the particle size, the smaller is the combustion chamber pressure.
2. The two-phase flow affects the flow field in the combustion chamber greatly. When the particle size increases, the gas speed increases, the pressure, total pressure and the gas density all decrease. When the particle speed decreases, the density increases. The effect of the particle size on the temperature of both gas and particle is very small.
3. In the combustion chamber the lag of the particle speed increases along the length of the duct, the lag of the temperature basically keeps constant. Besides, the particle speed lag is greater

than the temperature lag. When the particle size is small, the two-phase flow in the combustion chamber can be treated as the constant lag flow.

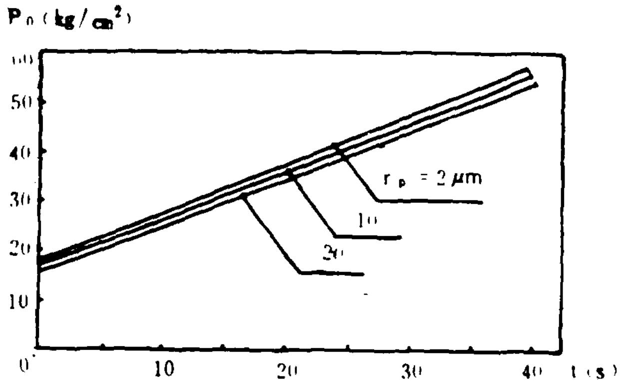

Figure 3. Pressure-Time Curve

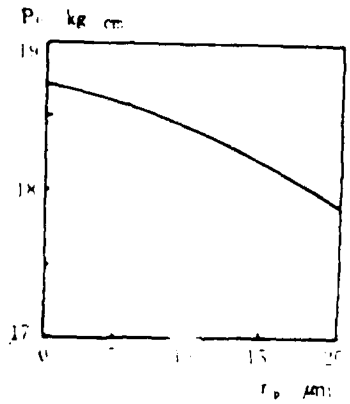

Figure 4. Effect of the particle size on P_o

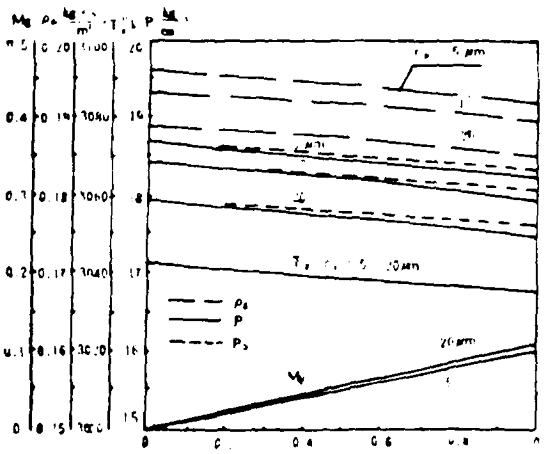

Figure 5. Distribution of gas parameters in the two-phase flow.

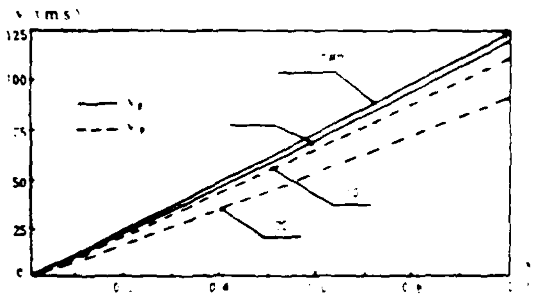

Figure 6. Speed distribution of the gas and the particle in two-phase flow.

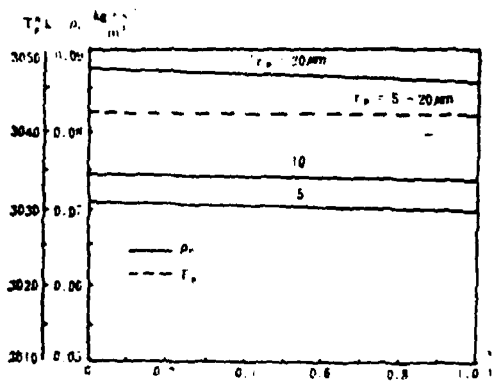

Figure 7. Distribution of the particle parameters in two-phase flow.

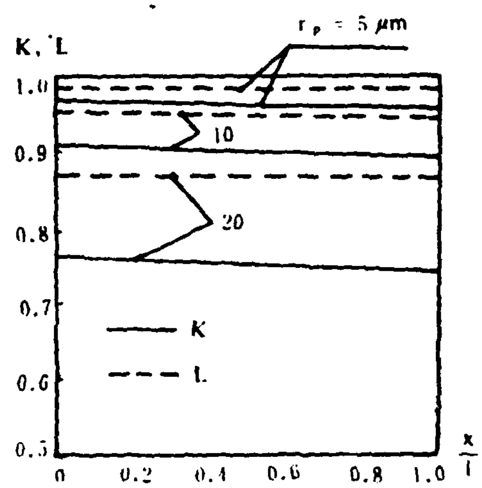

Figure 8. Particle speed lag factor and temperature lag factor distribution.

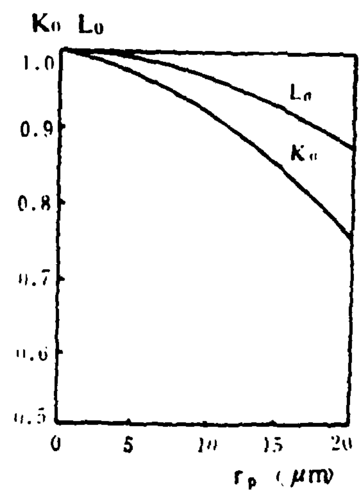

Figure 9. The effect of the particle size on the values of K_o, L_o.

REFERENCES

[1] AD 766 567, Chapter VI, 1973.

[2] Hoffman, Joe D.: Gas Dynamics, Volume II P53-66, 1977.

[3] 'Fundamentals of solid rocket engine design" (Vol. 1) Changsha Institute of Technology, 1976.

[4] Chang Xiangi: Unidimensional two-phase retarded flow in solid rocket engine combustion chamber. Journal of Astronautics, 1983, No. 4.

PRESSURE COUPLED RESPONSE FUNCTION OF SOLID PROPELLANTS INCLUDING THOSE WITH NEGATIVE PRESSURE EXPONENTS

XU Weng-an

SUMMARY

On the basis of the evidence presented, a steady state combustion model (1) of solid state propellents with negative pressure coefficient burn speed characteristics allows us to derive a new pressure response function formula. This can be used to explain pressure pairing phenomena for propellents whose combustion speed pressure exponents are zero, positive, and negative. The burning propellent is divided into two sections: the first section is a structure composed of oxidizing agent covered by molten binding agent and the corresponding binding agent surface. The other section is formed by uncovered oxidizer surface and remaining binding agent surface. This model is different from the various types of models in the past. In the combustion on the surface of the first type of section described above, consideration has been given to the oxidizer, under conditions in which it is covered by molten binding agent, so that it is considered to be in a state of opposed gasification and congealed phase reaction. Therefore, the real section of the pressure response function which is obtained, when the pressure exponent of the propellent steady state fuel speed is zero or has a negative value, is also capable of being a positive value. When we made use of the expression obtained for the pressure response function in experimentation with the propellent (S04-5A) and made qualitative calculations, the results of these calculations satisfactorily explain the phenomenon of propellents with negative pressure exponents still being unstable in combustion when most of the surface area of the oxidizer is covered by molten binder agent. This not only overcomes the weaknesses which all expressions for pressure response functions had in the past when used with negative pressure exponent propellents, but also, in a way, reflects the accuracy of the solid fuel propellent steady state combustion model (1) in its combustion speed characteristics for positive and negative pressure exponents.

Explanation of Symbols

$A \qquad \equiv \frac{E_{ox}}{R^{0}T_{s}}\left(1-\frac{T_{i}}{T_{s}}\right)$

A_{ox} Oxidizer Gasification Rate Indicator Prefactor

$$B \equiv \frac{2R^{\circ}T_{f}^{2}}{(T_{s}-T_{i})E_{f}}$$

B_{i} Indicator Prefactor in Oxidation Agent Equilibrium Evaporation Pressure Formula

$$C \equiv \frac{B_{i}\left(1+\frac{G}{1-G}\frac{W_{AP(g)}}{W_{G}}\right)}{P\exp\left(\frac{q}{R^{\circ}T_{s}}\right)}-1$$

c Specific Heat

$$D \equiv A+\lambda_{i}(AB-A)$$

(48

$$E \equiv \frac{C}{C+q/E_{ox}}\Omega+\lambda_{i}(AB-A)$$

E_{ox} Energy of Activation for Oxidizer Agent Gasification Reaction

E_{f} Energy of Activation for the Propellent Gas Phase Combustion Process

$$F \equiv \Omega+\lambda_{i}(AB-A)$$

G Mass Fraction of Oxidizer Agent for Completion of Condensation Phase Reaction

K Speed Constant for Gas Phase Reaction

m Mass Flow Rate

n Combustion Speed Pressure Exponent

p Pressure

Q_F Unit Mass Binder Decomposition Reaction Heat

Q_i Boundary Layer Reaction Heat of Unit Mass Oxidizer

q Heat of Evaporation for Unit Mass Oxidizer

q_g Heat Flow for Gas Phase Boundary Surface Flow

Q_g Amount of Heat Released by Unit Mass Gas Phase Reaction

q_r Rate of Release for the Heat of Purification from Boundary Surface Reaction

Q_r Real Section

R^0 Universal Gas Constant

R_P Pressure Response Function $\equiv \frac{\tilde{m}}{\bar{m}} / \frac{\tilde{p}}{\bar{p}}$

S $\equiv i\omega \frac{\rho\lambda}{\bar{m}^2 c} \equiv i\Omega$ (i is the imaginary number unit $\sqrt{-1}$)

T Temperature

T_f Absolute Temperature of the Propellent Flame

T_i Initial Propellent Temperature

T_s Propellent Surface Temperature

t Time

$W_{AP(g)}$ Gram molecular weight of oxidizer evaporation gas

W_G Gram Molecular Weight of Gaseous Products from Congealed Phase Oxidizer Reaction

x Distance

α Mass Fraction of Oxidizer in the Propellent

γ Surface Area Fraction Composed of Oxidizer Agent Surface Covered by Molten Binder Agent

λ Congealed and Solid Phase Heat Conduction Coefficient

ξ Nondimensional Distance $\equiv \frac{mc}{\lambda} x$

ρ Congealed and Solid Density

Ω Nondimensional Frequency $\equiv \frac{\rho\lambda}{m^2 c} \omega$

ω Angular Frequency

SUPERSCRIPTS

$-$ Steady State Value or Average Value

$'$ Perturbation Value

$\sim$ Complex Amplitude of Perturbation

I Parameters Corresponding to Area I

II Parameters Corresponding to Area II

SUBSCRIPTS

i Imaginary Section

r Real Section

I Parameters Corresponding to Area I

II Parameters Corresponding to Area II

s Boundary Surface, Value (Congealed Phase Side) for the Place Where $x=0$

1. Introduction

Sonic instability is the primary form of combustion instability of solid propellent rocket motors. Moreover, this type of sonic instability has as its primary source the combustion response of solid fuel propellents. Because of this, in the test construction of solid rocket motors, the sonic instability which they show is extremely important, and the theory and measurements associated with combustion response are indispensable. In linear sonic analysis, on sees shown whether or not a solid rocket motor will give a timely, consistent pressure perturbation enlargement, forming a sonically unstable fuel. In this type of analysis, the pressure response function must already be known. Therefore, the problem of solid propellent pressure response has received large amounts of research work in both the U.S. and the Soviet Union.

F.E.C. Culick (2) and N.S. Cohen (3) have already done excellent critiques of this problem. Concerning "flatbed" propellent pressure response functions, F.E.C. Culick and others (2) (4) have also done large amounts of research. However, the author recognizes that the steady state combustion model and several assumptions which form the basis of the research are still short on experimental data to support them. Moreover, several points of theory are still doubtful. For example, in order to explain the phenomenon of sonic vibrations in the combustion of flatbed propellents, we take the mass gasification rate for solid phase reaction areas and change it for use in the expression below:

$$m = A_s P^{n_s} e^{-\frac{E_s}{R^0 T_s}}$$

From this, we can derive the pressure response function formula:

$$R_p = \frac{nAB + n_s(\lambda - 1)}{\lambda + \frac{A}{\lambda} - (1 + A) + AB}$$

Moreover, when we use this relationship to compare with the results of experiments, we select $n_s = 1.0$. However, we know that, when the pressure exponent of the mass gasification rate for solid phase reaction areas is a positive value, the pressure exponent for its steady state combustion speed can hardly be zero. This article does not intend to make more criticism of these publications. We will present on the basis of a steady state model (1) of solid fuel propellents in terms of positive and negative pressure exponents for combustion speed characteristics, and derive a new pressure response function formula and force diagram. We will use them to make a complete explanation of the pressure pairing phenomenon which exists in various types of solid propellents when their combustion speed pressure exponents are zero, positive, and negative.

2, Physical-Chemical Model

In the same way as was the case with the corresponding steady state model (1), we select for use a one dimensional model and divide the combustion surface of the propellent into two sections. One section is composed of oxidizer agent surface covered by molten binder agent and the corresponding binder agent surface. Let us also stipulate that the fraction of surface area which it occupies out of the whole combustion surface is ν . The other section is then composed of oxidizer surface /50 which is not covered and the remaining binder agent surface. These two sections are respectively called, for short, Area I and Area II, as shown in Fig. 1. At the same time, we take the combustion process for each solid propellent area and simplify it into three stages, which respectively occur in three different phases (Fig. 2).

1) The solid phase area on the inside of the solid propellent, to which heat is applied, is gasified by the gas phase flame area with the congealed phase reaction area supplying the heat.

2) Within the congealed phase layer between the solid phase and the gas phase one sees the development of an oxidizer boundary layer reaction and binder agent heat of decomposition which are contained in the congealed phase reaction and the gasification reaction. In Area I, unlike Area II, one must consider the molten binder agent liquid layer which covers the surface of the oxidizer as well as the oxidizer underneath it as they exist in the congealed phase reaction related to gasification and its opposite process--opposed gasification.

3) In the gas phase one sees the occurrence of combustion processes which include dispersion, mixing, and chemical reaction.

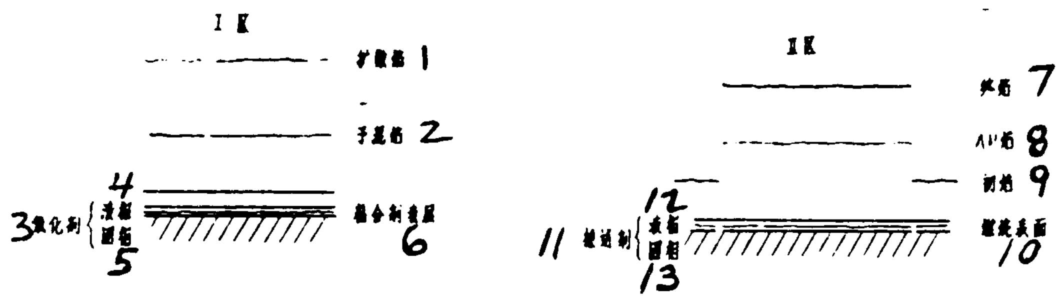

Fig. 1 One Dimensional Steady State Model
1. Dispersed Flame 2. Perturbed Flame 3. Oxydizer Agent 4. Liquid Phase 5. Solid Phase 6. Paired Agent Mixed Layer 7. End Flame 8. AP Flame 9. Initial Flame 10. Combustion Surface 11. Propellant 12. Liquid Phase 13. Solid Phase

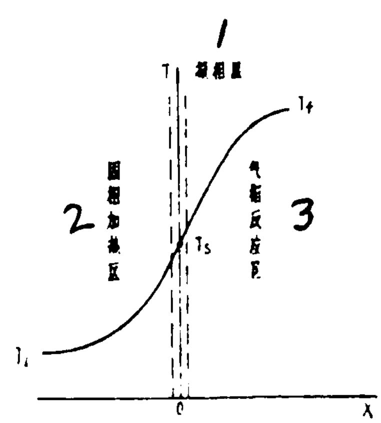

Fig. 2 A Simplified Two Dimensional Model 1. Congealed Phase Layer 2. Solid Phase Area of Increased Heat 3. Gas Phase Reaction Area

3, Mathematical Treatment

For the sake of convenience in the mathematical treatment, we first make the following assumptions:

1) The influence of heat damage is negligible.

2) The solid propellent is noncompressible, of a uniform qualtiy, and of the same nature in all directions.

3) The congealed phase layer between the solid phase and the gas phase is an infinitely thin plane. In this plane one sees occuring the oxidizer congealed phase reaction and the gasification reaction (Area I and Area II are different and each has its own rules of reaction). At the same time, one sees occuring the high temperature decomposition of binder agent. This plane is called the boundary surface.

(4) In the three solid, liquid, and gas phases discussed above, the specific heat is always a constant.

5) Gas phase reactions can be seen to be steady state processes.

6) The influence of congealed phase reactions on pressure disturbances is negligible. (51

7) When the amount of perturbation is sufficiently small, its second and higher order small amounts can all be neglected.

At the same time, in the same fashion as normal models, we choose for use a moving coordinate system. These coordinates take the instantaneous burn speeds of the propellents and move them into the solid phase area. In this way, the origin of the coordinate system can fall entirely on the solid-gas phase boundary surface.

Below we present the respective treatments for Area I and Area II.

Area I:

(1) Basic Equations

1) The unstable thermal conductivity equation in the solid phase heat addition area is:

$$\lambda \frac{\partial^2 T}{\partial x^2} - mc \frac{\partial T}{\partial x} = \rho c \frac{\partial T}{\partial t} \qquad (1)$$

2) When we consider the existence of molten boundary agent on the covering of oxidizer surface and the oxidizer under the covering as they affect congealed phase reactions and gasification reactions, from reference article (1), the mass gasification rate of propellent is:

$$m=\frac{1}{a}\cdot\frac{1}{1-G}A_{0x}\exp\left(-\frac{E_{0x}}{R^{0}T_{s}}\right)\left[1-\frac{P\exp\left(\frac{q}{R^{0}T_{s}}\right)}{B_{1}\left(1+\frac{G}{1-G}\frac{W_{AP(g)}}{W_{G}}\right)}\right] \quad (2)$$

3) If we assume a steady state, the mass combustion rate for the gas phase reaction area can be expressed as (5):

$$m=KP^{n}\exp\left(-\frac{E_{f}}{2R^{0}T_{f}}\right) \quad (3)$$

4) Energy equilibrium equation for the inside of the infinitely thin congealed phase layer:

The difference between the heat flow q_g from the gas phase combustion area and the heat flow $\lambda\frac{\partial T}{\partial x}\Big|_{x=0}$ transfered into the solid phase should equal the rate of heat release q_c, which is produced by the reaction in the congealed phase layer of the congealed phase and the gasification reaction, that is,

$$q_{g}-\lambda\frac{\partial T}{\partial x}\Big|_{x=0}=q_{c}$$

Moreover, using motion coordinates for explanation, $q_g=m[Q_g-c(T_f-T_s)]$, ,also, $q_c=m[aQ_s-(1-a)Q_F]$. In these equations, Q_g is the amount of heat released by the unit mass gas phase reaction. Q_s is the algebraic sum of the effective heats of the oxidizer agent congealed phase reaction and the gasification reaction. Q_F is the effective heat from the high temperature thermal decomposition of binder agent. If we substitute the equations above, we get

$$\lambda \frac{\partial T}{\partial x}\Big|_{x=0} + m[aQ_s - (1-a)Q_F - Q_g + c(T_f - T_s)] = 0 \tag{4}$$

(2) Linearization Treatment:

1) First, we carry out a linearization treatment of equation (1). We postulate:

$$\left.\begin{array}{l} m(t) = \bar{m} + R_e\{\tilde{m} e^{i\omega t}\} \\ T(x,\ t) = \bar{T}(x) + R_e\{\tilde{T}(x) e^{i\omega t}\} \end{array}\right\} \tag{5}$$

If we substitute in equation (1), and eliminate the high order small quantities, as well as making use of the steady state condition

$$\lambda \frac{d^2 \bar{T}}{dx^2} - \bar{m} c \frac{d\bar{T}}{dx} = 0 \tag{6}$$

then, equation (1) changes to become:

$$R_e\left\{\lambda \frac{d^2 \tilde{T}}{dx^2} e^{i\omega t}\right\} - R_e\left\{\tilde{m} e^{i\omega t} c \frac{d\bar{T}}{dx}\right\} - R_e\left\{\bar{m} e^{i\omega t} c \frac{d\tilde{T}}{dx}\right\} = R_e\{\rho c \tilde{T} i\omega e^{i\omega t}\},$$

Because these forms are set up for all times t, therefore, one has only

$$\lambda \frac{d^2 \tilde{T}}{dx^2} - \tilde{m} c \frac{d\bar{T}}{dx} - \bar{m} c \frac{d\tilde{T}}{dx} = i\omega\rho c \tilde{T} \tag{7}$$

Set

$$\left.\begin{aligned} \xi &\equiv \frac{\bar{m} c}{\lambda} x \\ S &\equiv i\omega \frac{\rho c}{\bar{m}^2 c} = i\Omega \end{aligned}\right\} \tag{8}$$

Then equations (6) and (7) can respectively be written

$$\frac{d^2 \bar{T}}{d\xi^2} - \frac{d\bar{T}}{d\xi} = 0 \tag{9}$$

$$\frac{d^2 \tilde{T}}{d\xi^2} - \frac{d\tilde{T}}{d\xi} - S\tilde{T} = \frac{\tilde{m}}{\bar{m}} \frac{d\bar{T}}{d\xi} \tag{10}$$

2) In the same way, in the case of equation (2), one can set

$$\left.\begin{aligned} m &= \bar{m} + m' = \bar{m} + R_e\{\tilde{m} e^{i\omega t}\} \\ T_s &= \bar{T}_s + T'_s = \bar{T}_s + R_e\{\tilde{T}_s e^{i\omega t}\} \\ P &= \bar{P} + P' = \bar{P} + R_e\{\tilde{P} e^{i\omega t}\} \end{aligned}\right\} \tag{11}$$

Moreover, one can use the steady state condition

$$\bar{m} = \frac{1}{\alpha} \cdot \frac{1}{1-G} A_{os} \exp\left(-\frac{E_{os}}{R^0 \bar{T}_s}\right) \left[1 - \frac{\bar{P} \exp\left(\frac{q}{R_s \bar{T}_s}\right)}{B_1 \left(1 + \frac{G}{1-G} \frac{W_{AP(ST)}}{W_G}\right)}\right]$$

Division with equation (2) gives one

$$1+\frac{m'}{m}=\exp\left(\frac{E_{0z}}{R^0T_0}\cdot\frac{T_0'}{T_0}\right)\frac{C+1-\left(1+\frac{P'}{P}\right)\exp\left[\frac{-q}{R^0T_0}\cdot\frac{T_0'}{T_0}\right]}{C} \tag{12}$$

In the equation

$$C\equiv\frac{B_1\left(1+\frac{G}{1-G}\,\frac{W_{AP(0)}}{W_C}\right)}{P\exp\left(\frac{q}{R^0T_0}\right)}-1$$

Also, because of the fact that $\frac{E_{0z}}{R^0T_0}\cdot\frac{T_0'}{T_0}$ and $\frac{q}{R^0T_0}\cdot\frac{T_0'}{T_0}$ are both very small $\left(\frac{E_{0z}}{R^0T_0}\right.$ and $\frac{q}{R^0T_0}$ are both of the order of magnitude of 10). Moreover, $\frac{T_0'}{T_0}$ is then in the range $10^{-3}\sim10^{-2}$. Therefore, one has

$$\exp\left(\frac{E_{0z}}{R^0T_0}\cdot\frac{T_0'}{T_0}\right)\approx1+\frac{E_{0z}}{R^0T_0}\cdot\frac{T_0'}{T_0}$$

$$\exp\left(\frac{-q}{R^0T_0}\cdot\frac{T'}{T_0}\right)\approx1-\frac{q}{R^0T_0}\cdot\frac{T_0'}{T_0}$$

Substituting in equation (12) and eliminating the smaller quantities of higher order, one, then, obtains

$$\frac{m'}{m}=\frac{E_{0z}}{R^0T_0}\cdot\frac{T_0'}{T_0}-\frac{\frac{P'}{P}-\frac{q}{R^0T_0}\,\frac{T_0'}{T_0}}{C}$$

As above, because of the fact that all of the equivalent forms for times should be set up, one, consequently has

(53

$$\frac{\bar{m}}{m}=\frac{E_{0z}}{R^0T_0}\left[\frac{C+\frac{q}{E_{0z}}}{C}\,\frac{\bar{T}_0}{T_0}-\frac{R^0T_0}{CE_{0z}}\,\frac{\bar{p}}{P}\right] \tag{13}$$

3) After one carries out the same type of linearization treatment on equation (3), one obtains:

$$\frac{\tilde{T}_f}{T_f}=\frac{\frac{\tilde{m}}{m}-n\frac{\tilde{p}}{p}}{\frac{E_f}{2R^0T_f}} \tag{14}$$

4) In the same way, equation (4) can be changed to become:

$$\left(\frac{d\tilde{T}}{d\xi}\right)_s+(\tilde{T}_f-\tilde{T}_s)=\frac{\tilde{m}}{m}\left(\frac{dT}{d\xi}\right)_s \tag{15}$$

(3) Solution of Equations

Because equation (9) and its boundary condition are:

$$\frac{d^2T}{d\xi^2}-\frac{dT}{d\xi}=0$$

$$\begin{cases}\xi=-\infty \text{ time } T=T_i\\ \xi=0 \quad \text{ time } T=T_s\end{cases}$$

it follows that its solution is obviously $T=T_i+(T_s-T_i)e^{\xi}$. Moreover, $\frac{dT}{d\xi}=(T_s-T_i)e^{\xi}$. If we take this expression and substitute it into equation (15), we then get

$$\left(\frac{d\tilde{T}}{d\xi}\right)_s=-\left(\tilde{T}_f-\tilde{T}_s\right)+T_s\left(1-\frac{T_i}{T_s}\right)\frac{\tilde{m}}{m} \tag{16}$$

Moreover, if we substitute equation (13) and equation (10), equation (10) changes into

$$\frac{d^2\tilde{T}}{d\xi^2}-\frac{d\tilde{T}}{d\xi}-S\tilde{T}=\frac{E_{0x}}{R^0}\left(1-\frac{T_i}{T_s}\right)\left[\left(\frac{C+\frac{q}{E_{0x}}}{C}\right)\frac{\tilde{T}_s}{T_s}-\frac{R^0T_s}{CE_{0x}}\frac{\tilde{p}}{p}\right]e^{\xi}$$

Its boundary conditions are:

$$\begin{cases} \xi = -\infty \text{ time } \mathcal{T} = 0 \\ \xi = 0 \text{ time } \mathcal{T} = \mathcal{T}_{,} \end{cases}$$

Therefore a general solution for the equation is:

$$\mathcal{T} = c' e^{\lambda \xi} - \frac{A}{S}\left[\frac{C + \frac{q}{E_{0x}}}{C} - \frac{T_{,}}{T_{,}} \frac{R^{0}T_{,}}{CE_{0x}} \frac{P}{P}\right]\mathcal{T}_{,} e^{\xi}$$

In the equations $A \equiv \frac{E_{0x}}{R^{0}T_{,}}\left(1 - \frac{T_{i}}{T_{,}}\right)$. Moreover, λ is then determined from the characteristic equation $\lambda^{2} - \lambda - S = 0$. Because, when $\xi = -\infty$, $\mathcal{T} = 0$; therefore, one only has $\lambda = (1 + \sqrt{1 + 4S})/2$ as a characteristic limit. Again, from the boundary condition $\xi = 0$, when $\mathcal{T} = \mathcal{T}_{,,}$, it is possible to obtain a solution to the equation as follows:

$$\mathcal{T} = \mathcal{T}_{,}\left[e^{\lambda \xi} + \frac{A}{S}\left(\frac{C + \frac{q}{E_{0x}}}{C} - \frac{T_{,}}{T_{,}} \frac{R^{0}T_{,}}{CE_{0x}} \frac{P}{P}\right)\left(e^{\lambda \xi} - e^{\xi}\right)\right]$$

Substituting in equation (16), one then obtains:

(54

$$\lambda + \frac{A}{S}\left(\frac{C + \frac{q}{E_{0x}}}{C} - \frac{T_{,}}{T_{,}} \frac{R^{0}T_{,}}{CE_{0x}} \frac{P}{P}\right)(\lambda - 1)$$
$$= \left(1 - \frac{T_{i}}{T_{,}}\right)\left(\frac{T_{,}}{T_{,}}\right)^{-1} \frac{\dot{m}}{\dot{m}} - \left[\frac{T_{l}}{T_{l}} \cdot \frac{T_{l}}{T_{,}} \cdot \left(\frac{T_{,}}{T_{,}}\right)^{-1} - 1\right] \qquad (17)$$

From equation (13), one has

$$\left(\frac{\tilde{T}_s}{\bar{T}_s}\right)^{-1} = \frac{E_{0x}}{R^0 \bar{T}_s} \cdot \frac{C+\frac{q}{E_{0x}}}{C\frac{\tilde{m}}{\bar{m}}+\frac{\tilde{P}}{\bar{P}}} \tag{18}$$

If one takes equations (14) and (18) and substitutes them with equation (17), one then obtains: -

$$\lambda+\frac{A}{S}\left(\frac{C+\frac{q}{E_{0x}}}{C}-\frac{\frac{\tilde{P}}{\bar{P}}}{C}\cdot\frac{C+\frac{q}{E_{0x}}}{C\frac{\tilde{m}}{\bar{m}}+\frac{\tilde{P}}{\bar{P}}}\right)(\lambda-1)$$

$$= A\frac{\tilde{m}}{\bar{m}}\cdot\frac{C+\frac{q}{E_{0x}}}{C\frac{\tilde{m}}{\bar{m}}+\frac{\tilde{P}}{\bar{P}}}-\left[\frac{\frac{\tilde{m}}{\bar{m}}-n\frac{\tilde{P}}{\bar{P}}}{\frac{E_f}{2R^0\bar{T}_f}}\cdot\frac{\tilde{T}_f}{\tilde{T}_s}\cdot\frac{\frac{C+\frac{q}{E_{0x}}}{C\frac{\tilde{m}}{\bar{m}}+\frac{\tilde{P}}{\bar{P}}}}{\frac{R^0 T_s}{E_{0x}}}-1\right]$$

If we make $B \equiv \frac{2R^0 T_f^2}{(T_s - T_i)E_f}$, and we make use of the pressure response function definition $R_p \equiv \frac{\tilde{m}}{\bar{m}} \Big/ \frac{\tilde{P}}{\bar{P}}$, then, the above equation can be arranged so that:

$$R'_p = \frac{nAB - \frac{\lambda-1}{C+q/E_{0x}}}{\frac{A}{\lambda} - A + AB + \frac{C}{C+q/E_{0x}}(\lambda-1)}$$

Area II:

Based on a method similar to the one above, we only take basic equation (2) and change it to be $m = A_{0x}\exp\left(-\frac{E_{0x}}{R^0 T_s}\right)$. It is then possible to obtain an expression for the pressure response function for Area II(5):

$$R_p^{II}=\frac{nAB}{\frac{A}{\lambda}-A+AB+(\lambda-1)}$$

Again, on the basis of the normal assumption that there is a direct proportion between combustion surface gain and combustion surface area, the pressure response function for the entire combustion surface formed by Area I and Area II should be:

$$R_P=\gamma\frac{n_IA_IB_I-\frac{\lambda-1}{C+q/E_{0x}}}{\frac{A_I}{\lambda}-A_I+A_IB_I+\frac{C}{C+q/E_{0x}}(\lambda-1)}+(1-\gamma)\frac{n_{II}A_{II}B_{II}}{\frac{A_{II}}{\lambda}-A_{II}+A_{II}B_{II}+(\lambda-1)}$$

Actually, the imaginary section is:

(55

$$(R_P)_r=\gamma\frac{\lambda_rn_IA_IB_ID+\left(\lambda_in_IA_IB_I-\frac{\Omega}{C+q/E_{0x}}\right)E}{D^2+E^2}$$
$$+(1-\gamma)\frac{n_{II}A_{II}B_{II}(\lambda_rD+\lambda_iF)}{D^2+F^2}$$

$$(R_P)_i=\gamma\frac{-\lambda_rn_IA_IB_IE+\left(\lambda_in_IA_IB_I-\frac{\Omega}{C+q/E_{0x}}\right)D}{D^2+E^2}$$
$$+(1-\gamma)\frac{n_{II}A_{II}B_{II}(\lambda_iD-\lambda_rF)}{D^2+F^2}$$

In these equations,

$$D \equiv A+\lambda_r(AB-A), \quad E \equiv \frac{C}{C+q/E_{0s}}\Omega+\lambda_i(AB-A),$$

$$F \equiv \Omega+\lambda_i(AB-A);$$

$$\lambda_r=\frac{1}{2}\left\{1+\sqrt{\frac{1}{2}\left[1+(1+16\Omega^2)^{\frac{1}{2}}\right]^{\frac{1}{2}}}\right\}$$

$$\lambda_i=\frac{1}{2}\sqrt{\frac{1}{2}\left[-1+(1+16\Omega^2)^{\frac{1}{2}}\right]^{\frac{1}{2}}}$$

4. Results of Calculations and Discussion

Making use of the steady state model(1), the various results of intitial calculations on SO4-5A experiments (Table 1) form the initial data to substitute into the formula for the real section of the pressure response function, yielding results such as those shown in Fig. 3.

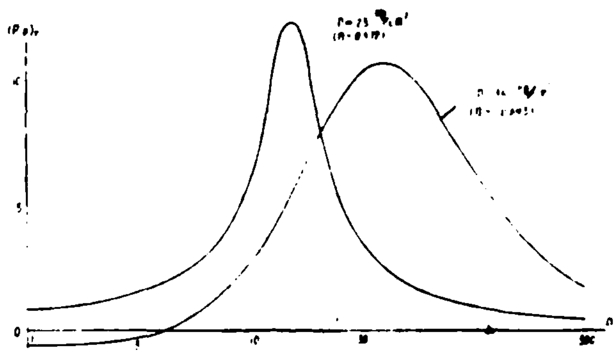

Fig. 3 The Real Portion of Two Low Pressure Response Functions for SO4-5A

The formulas obtained and the results of calculations all clearly show that the real sections of pressure response functions for "plateau" and "mesa" propellants whose pressure exponents are zero or negative are all capable of being positive values larger than zero within quite a large range of frequencies. From the standpoint of theory, this explains very well facts associated with severe phenomena of unstable combustion and the existence of these two types of propellents(4),(6),(8). Moreover, just as this author calculated in reference (1), due to the fact that the abnormal combustion of oxidizer covered with molten binder agent takes the place of partial shut down, in this way, under the pressure associated with the existence of widespread covering, it is, on the contrary, easy to see the appearance of the results of self-e xcited oscillation . It is then possible to give a reasonable explanation. (56

参 1 数	单 2 位	数 3 值	参 1 数	单 2 位	算例 4 1	算例 4 2
B_1	kg/cm²	3.48×10^5	P	kg/cm²	23	35
C	Cal/g·°K	0.3	G		0.3	0.2
E_{ox}	Cal/mole	2.2×10^4	γ		0.6	0.8
E_f	Cal/mole	6.0×10^4	n		0.572	−0 693
q	Cal/mole	2.08×10^4	T_{sI}	°K	1038.6	1098.8
T_f	°K	2900	n_I		0.75	−0.783
T_i	°K	293	T_{sII}	°K	1086.6	1108.0
$W_{AP(g)}$	g/mole	117.5	n_{II}		0.486	0.424
W_c	g/mole	28.4				
λ	Cal/cm·sec·°K	0.3×10^{-3}				
ρ	g/cm³	1.665				

Table 1 1. Parameter 2. Unit 3. Numerical Value 4. Sample Calculation

What the dotted line in Fig. 3 shows is that, in reference (1), S04-5A propellant, with a large surface area covered and a pressure of $P=23\text{kg/cm}^2$, in experiments with the "T" type engine, shows the appearance of self-excited oscillation. The frequencies involved correspond to the real section values of the response functions for quite high pressures. Because of this, the appearance of self-excited oscillation in these experiments cannot be considered surprising.

Most of the results discussed above were obtained through analysis in Area I. This was done through the use of our steady state model and with consideration given to the covering of the oxidizer surface with molten binder agent and to the existence of a congealed phase reaction as well as opposed gasification. Because of this, the theoretical formula derived for the pressure response function can not only overcome the deficiency associated with the fact that the pressure response function formulas we already have cannot be used with negative propellent pressure exponents, but also, in one respect, it reflects the vitality of the stable state combustion model(1) for solid state propellents, which presents the combustion speed characteristics for positive and negative pressure exponents.

The formula which is derived when the covered surface area fraction γ is zero, then becomes the "two parameter formula" for propellents with binder agents which are difficult to melt:

$$R_p = \frac{nAB}{\lambda + \frac{A}{\lambda} - (1+A) + AB}$$

Taking use of the unified expression we already have for the "gas phase quasi-steady state, uniform propellent unidimensional model"(2), this article consequently derives a formula which is capable of having even broader applicability.

This article, before deriving this formula, made no small number of empirically quite significant assumptions. For example, the assumption that the congealed phase layer which gives rise to the congealed phase reaction and the gasification reaction is an infinitely thin plane is certainly not a good approximation(2). The assumption that the gas phase assumes a steady state has an error less than 10% only when the frequencies are smaller than 10,000 Hertz(2)(5). The compressiblity of propellents also has an influence on response functions which is within 10%(9). Heat radiation losses, under certain conditions, also have an obvious influence on response functions(10)(11). As far as congealed phase reactions are concerned, in our stable state model, they are basically pressure functions(1). However, we also conveniently saw from our mathematical treatment, that, when their influence on pressure diminishes , error is, naturally, even more unavoidable. Although, except for congealed phase reaction problems, the majority of assumptions are obvious, they are also universal in their application. However, this explains the fact that the formulas derived above are still awaiting refinement.

At the same time, formulas derived on the assumption of homogeneity can, of course, only be used in situations where one has homogeneity. However, due to the fact that propellant impurities have already been (57
used by several scholars (12) in methods such as the one that follows; that is, taking a multi-mode composite propellant and viewing it as a finely dispersed oxydizer granule/fuel "surface match up" of random arrangement. When one assumes that each "pairing" is mutually indpendent, then it also becomes possible to take the propellant surface and rearrange it into a family of hypothetically dispersed units of propellant. This is what is called a hypothetical propellant. And, the pressure responses of these hypothetical fuels are calculated using formulas deduced from homogeneous theory. Moreover, from this one obtains the pressure response for the whole composite propellant. Just as is pointed out in reference (3), although this method has the drawbacks of two different models in its application, it is still currently being followed. Because of this, this model certainly does not fail to explain pressure pairing problem values for composite solid propellents because of its adoption of a homogeneity hypothesis.

5, Conclusions

1) Making use of a steady state combustion model for positive and negative pressure exponent combustion speed characteristics for solid propellants, we deduced a new pressure response function formula. This formula explains, in a reasonable way, phenomena associated with unstable combustion which exists in all solid propellants with positive, negative and zero pressure exponents.

2) In the same way which was the case with the forming of a model for steady state combustion, in the combustion of propellants, the phenomenon of molten binder agent covering oxidizer surface area should also be considered in the forming of a model for unstable combustion of solid propellants.

3) Using the unusually regular combustion of the congealed phase reaction and opposed gasification covered by molten binder agent to replace localized shut down is a precise and necessary method. This is true not only for steady states, but for non-steady states as well.

4) The model presented in this article is still awaiting further experimental testing and perfecting.

REFERENCES

[2] Culick, F. E. C.: A Review of Calculations for Unsteady Burning of a Solid Propellant, AIAA J. Vol. 6, No. 12, 1968.

[3] Cohen, N. S.: Response Function Theories that Account for Size Distribution Effects-A Review, Paper AIAA 80-1123.

[4] Beckstead, M. W. and Culick, F. E. C.: A Comparision of Analysis and Experiment for Solid Propellant Combustion Instability, AIAA J. Vol. 9, No. 1, 1971.

[6] Culick, F. E. C.: Calculation of the Admittance Function for a Burning Surface, Astronautics Acta, Vol. 13, 1967.

[7] Kuman, R. N. and Culick, F. E. C.: Role of Condensed Phase Details in the Oscillatory Combustion of Composite Propellants, Paper AIAA 73-218.

[8] Cohen, N. S.: Combustion Response Modeling for Composite Solid Propellants, JPL/AFRPL-76-F.

[9] Bird, J. F., et al.: Effect of Solid Propellant Compressibility on Combustion Instability, Journal of Chemical Physics Vol. 32, May 1960.

[10] Cantrell, R. H., McClure, F. T. and Hart, R. W.: Effects of Thermal Radiation on the Acoustic Response Function of Solid Propellants, AIAA J. Vol. 3, No. 3, 1965.

[11] Cantrell, R. H., Hart, R. W. and McClure, F. T.: Linear Acoustic Gains and Losses in Solid Propellant Rocket Motors, AIAA J. Vol. 2, No. 6, 1964.

[12] Condon, J. A., and Osborn, J. R.: The Effect of Oxidized Particle Size Distribution on the Steady and Nonsteady Combustion of Composite Propellants, AD/A-056892.

(1) XU Wen-gan, LI Bao-xuan, WANG Ke-xiu: "Steady State Combustion Model for Composite Solid State Propellants Containing Negative Pressure Exponents," Astronautics Journal, 1983, No. 3

(5) XIE An-hu: "Linear Theory for the Unstable Combustion of Solid Fuel Rocket Motors", The Xi Bei Industrial College Journal for Scientific and Technical Material, No. 487, 1977.

(59

THE ANALYSIS AND CALCULATION FOR THE DYNAMIC CHARACTERISTICS OF THE OMNI-AXIAL MOVABLE FLEXIBLE JOINT NOZZLE

YANG Shi-xue

SUMMARY

In this article, under simulated engine combustion chamber pressure conditions, we carry out an analysis of and calculations for the dynamics of the omni-axial rotation of flexible jet nozzles. The important contents include: analytical calculations of measured data; analytical calculations for the center of instantaneous oscillation of jet nozzles; and, calculations of the moments of force of oscillation. Besides this, we also calculated the parameters that follow: the angle of oscillation and angular velocity of jet nozzles; azimuth angles of oscillation; the length of operating tubes; eccentricity of thrust; and, axial and radial displacement of jet nozzles under differing pressures of contents, etc.

This method of calculation, after having appropriately resolved the problem of installing telemetry pickups, is still suitable for use with hot test beds and is also suitable for calculations and measurements under conditions of static oscillation of flexible jet nozzles.

1, Calculations of Adjustments in the Amounts of Displacement and Angles of Oscillation

(1) Selection of Measuring Equipment and Coordinate System

The apparatus for measuring simulated axial oscillation of flexible jet nozzles is as shown (Fig. 1). The flexible connector head connects respectively with the end ring and the lower flat plate. They and the container shell body together form a sealed high pressure vessel. To the bottom flat plate is firmly attached a rod (simulating the jet nozzle). Its axis line and the axis line of the flexible connector head are congruent. Its point of contact on the Z plate is the origin of the coordinate system O (At this time the content pressure is zero.) The axis OZ is then congruent with the axis line of the rod.

The top end of the rod and the axis line are installed at right angles to the flat plate, which is called the Z plate. The axial line of the displacement sensor Z_1 is congruent with the axis line of the rod. The direction and amount of thrust are controlled by actuator tubes 1 and 2, which are respectively positioned in planes OXZ and OYZ. In this way a fixed coordinate system $OXYZ$

is then established. Two flat plates are installed on the rod. They are respectively perpendicular to the X axis (called the X plate) and the Y axis (called the Y plate). Displacement sensors X_3, X_2, X_1 and Y_2, Y_1 are respectively perpendicular to the X plate and the Y plate. Moreover, lines extending from X_2 and Y_2, and X_1 and Y_1 connect respectively with two points on the Z axis. Their points of intersection, with coordinates in these dimensions, are $(O,O,-Z_2),(O,O,-Z_1)$. An extension of the X_3 axis line of the displacement sensor intersects with the OZY coordinate plane at point $(O,-Y_0,-Z_2)$. The distance from the X plate and the Y plate to the coordinate point is R in both cases. The other two displacement sensors H_1 and H_2 respectively measure the two actuator tubes fixed to rod points Q_1 and Q_2 in terms of the amount of axial displacement caused by elastic deformations of the vessel.

Besides this, the radius of measurement contact heads for displacement sensors X_3, X_2, X_1, Y_2, Y_1 is R_0 in all cases. The radius of the measurement contact head for sensor Z_3 may be selected at will. Let this value be R_1. The rest of the installation constants and structural constants are as shown in the Figure.

F_1 (or P_1), and F_2 (or P_2) are activating forces (or pressure differential) sensors.

(2) Analysis of Displacement Sensor Measurement Data

Among the eight displacement sensors, except for the measurement data from H_1 and H_2 which there is no need to correct, the measured data obtained from the other six sensors certainly does not perfectly reflect the amount of displacement in the oscillation of the rod. This is due to the reasons set out below. (60

(1) The measuring contact head of the sensors is a hemisphere. According to changes in the angle of oscillation, contact points experience displacement along the hemisphere, introducing an additional amount of displacement.

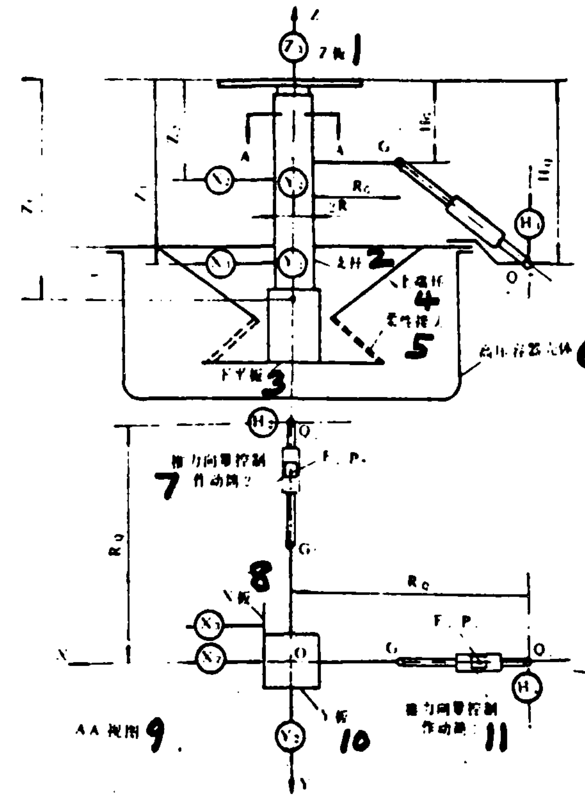

Fig. 1 Schematic Diagram of Test Equipment 1. Plate 2. Rod 3. Lower Flat Plate 4. Upper Compression Ring 5. Flexible Contact Head 6. High Pressure Container Shell 7. Actuator Tube 2 for Controlling the Direction and Amount of Thrust 8. Plate 9. Diagram 10. Plate 11. Actuator Tube 1 for Controlling the Direction and Amount of Thrust

(2) The measurement contact heads for the various displacement sensors X_3、X_2、X_1、Y_2、Y_1 and the contact points of the experimental measurement plates are at a distance from contact points on the rod axis line X_3 and from the symmetrical surface of the rod so that the distance varies with changes in the angle of oscillation.

(3) Because of the fact that the axis lines of X, Y, and Z rotate at the same time, their mutual influences cause plates X and Y to correspond to the slant which occurs in the sensors. This introduces an amount of non-displacement in the sensors.

(3) Adjustment Calculations for Angle of Oscillation and Amount of Displacement

Let the angles of rotation for the axis lines X, Y, and Z be β, α, θ. In order to simplify analysis and calculations, we make use of the geometrical principle of superposition to make a two step calculation. After that, we superimpose. That is, first we make calculations for the situation in which $\alpha \neq 0$ and $\beta \neq 0$, with $\theta = 0$. Then, we make the calculations for the situation in which $\alpha \neq 0, \beta \neq 0$ and $\theta \neq 0$.

(1) Adjustment Calculations for the Situation in Which $\alpha \neq 0, \beta \neq 0$ and we assume $\theta = 0$.

There are four types of factors in omni-axial oscillation which cause adjustments to the displacements measured by the displacement sensors: (a) $\alpha > 0, \beta < 0$; (b) $\alpha < 0, \beta < 0$; (c) $\alpha < 0, \beta > 0$; (d) $\alpha > 0, \beta > 0$. Formula derivation brings up one type of situation.

Eccentric rotation of the axis line within the first apparent limit $\alpha > 0, \beta < 0$.

If we assume that the cross section of a rod is a square 2R on a side, then, Fig. 2 is a cubic diagram of angle α and angle β of the deflection. Fig. 3 is a horizontal projection diagram corresponding to it.

Definition: The plane which holds the displacement sensors X_2 and Y_2 (or X_1 and Y_1) is the horizontal plane of test measurements. The same rod cross section used in it is reprsented by $\square EFGH$. If we assume that axis line Y rotates through angle α and axis line X then rotates through angle β, the change in the horizontal plane of test measurements is: square $\square E_0F_0G_0H_0 \xrightarrow{\alpha}$ elongated square $\square E'F'G'H' \xrightarrow{\beta}$ quadrilateral $\square EFGH$. This corresponds to a change in the contact point of the experimental measurement head of the X displacement sensor: $A_0 \to A_1 \to A_2$. (61

At point A_0: $\alpha = 0, \beta = 0$. X sensor measurements give as a displacement amount $X_0 = 0, A_0O = R$.

At point A_1 $\alpha > 0, \beta = 0$. The measured amount of displacement is X'. The actual amount of displacement is $X = O_1O$. One of the additional amounts of displacement is:

$$A_1O_1 - A_0O = R/\cos\alpha - R$$

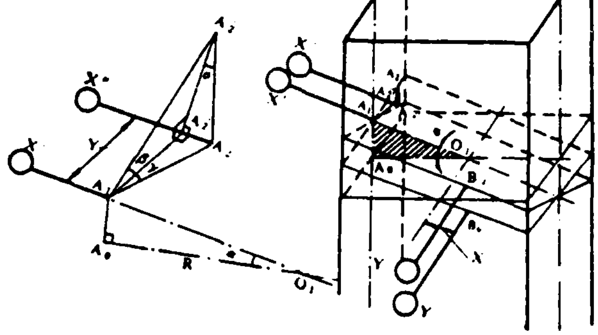

Fig. 2 Cubic Diagram of the Horizontal Test Measurement Plane When $\alpha > 0, \beta < 0, \theta = 0$

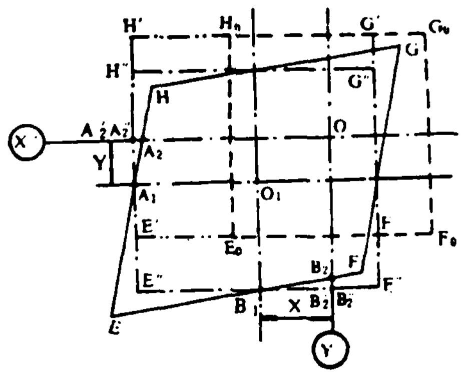

Fig. 3 Plane Diagram of the Test Measurement Plane When $\alpha > 0, \beta < 0, \theta = 0$

From the diagrams it is possible to see four amounts of additional displacement caused by the displacement of the contact points on the contact heads: $A_0A_0' = O'A_0' - O'A_0 = R_0/\cos\alpha - R_0$

$$X' = X + (R + R_0)(1/\cos\alpha - 1) \qquad (1)$$

At point A_1 : $\alpha > 0, \beta < 0$. Let the numerical data measured by the sensor be X'' . From Fig. 2 or Fig. 3 it is easy to see that the value of the difference between X'' and X' is $A_1''A_2$. These are three of the amounts of additional displacement caused by angle β on sensor X . From Fig. 2 we obtain the set of relationships set out below:

From $Rt\Delta A_1A_1'A_1''$ we get: $A_1'A_1'' = A_1A_1''\,\mathrm{tg}\,\beta = Y\,\mathrm{tg}\,\beta$

From $Rt\Delta A_2A_1'A_1''$ we get: $A_1''A_2 = A_1'A_1''\,\mathrm{tg}\,\alpha = Y\,\mathrm{tg}\,\alpha\,\mathrm{tg}\,\beta$ (2)

From $Rt\Delta A_1A_2A_1''$ we get: $A_1''A_2 = A_1A_1''\,\mathrm{tg}\,r = Y\,\mathrm{tg}\,r$ (3)

Compared with equation (2), equation (3) has: $r = \mathrm{arctg}[\mathrm{tg}\,\alpha \cdot \mathrm{tg}\,\beta]$ (4)

Because $A_1''A_2 = Y\,\mathrm{tg}\,r < 0$, we also give consideration to satisfying the geometrically equivalent relationship, and we then have:

$$X'' - A_1''A_2 = X' \qquad (5)$$

After we now do some more analysis of the deflection angle β , the four additional amounts of displacement which are induced in the displacements of the contact points on the measuring contact head of displacement sensor X can be seen from Fig. 4. The contact point moves from point A_1 to point A_2 : that is, it rotates through angle $\angle A_1'O''A_2 = r, O''A_1 = R_0\cos\alpha$. Because of this, there is always a positive amount of increase:

$$R_0\cos\alpha(1/\cos r - 1) \qquad (6)$$

When one combines this with equations (1)(2)(5)(4)(6) one gets:

$$X = X'' - Y\,\mathrm{tg}\,r - (R + R_0)\left(\frac{1}{\cos\alpha} - 1\right) - R_0\cos\alpha\left(\frac{1}{\cos r} - 1\right) \qquad (7)$$

Below, when we make adjustment calculations for the amount of displacement measured by the Y direction displacement sensor. We similarly have:

At point B_0 : $Y=0 \quad B_0O=R$

At point B_1 $\quad Y'=Y+(R+R_0)\left(\frac{1}{\cos\beta}-1\right)$ (8)

At point B_2 : $B_2'B_2=X\,\mathrm{tg}\,r$

(62

$\because X\,\mathrm{tg}\,r<0$, it satisfies the equivalent relationship

$$\therefore \quad Y''+B_2'B_2=Y'$$

$$Y''-X\,\mathrm{tg}\,r=Y' \tag{9}$$

The additional amount of displacement caused by the angle α is:

$$R_0\cos\beta(1/\cos\alpha-1) \tag{10}$$

From the various equations (8)(9)(10) one then obtains:

$$\dot{Y}=Y''-X\,\mathrm{tg}\,r-(R+R_0)(1/\cos\beta-1)-R_0\cos\beta(1/\cos r-1) \tag{11}$$

(2) Calculations to Adjust the Amount of Displacement When the Angles α,β,θ Are Simultaneously Not Zero

As far as an ideally flexible contact head is conerned, one has only the times when the azimuth angle of oscillation ψ_s is 45 degrees and 225 degrees , making use of forces, the combined force of which crosses over the axis of the jet tube. In the case of oscillations with other azimuth angles, making use of forces the combined force of which does not at all cross the axis of the jet tube,adds an additional moment of force to the axis line of the jet tube. In this way,the jet tube rotates around the Z axis line, the angle of which is designated θ . During omni-axial oscillation, it is only possible for the angle θ to be positive or negative. If one gives consideration to α,β , the overall influencing factors can be grouped into six types of situations, that is,

$0°=\psi_s<45°$	$\theta<0,(\alpha>0,\beta<0)$
$45°<\psi_s\leqslant 90°$	$\theta>0,(\alpha>0,\beta<0)$
$90°<\psi_s\leqslant 180°$	$\theta>0,(\alpha<0,\beta<0)$
$180°<\psi_s\leqslant 225°$	$\theta>0,(\alpha<0,\beta>0)$
$225°<\psi_s\leqslant 270°$	$\theta<0,(\alpha<0,\beta>0)$
$270°<\psi_s\leqslant 360°$	$\theta<0,(\alpha>0,\beta>0)$

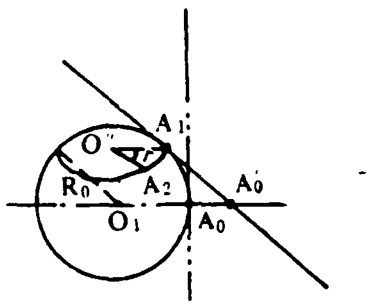

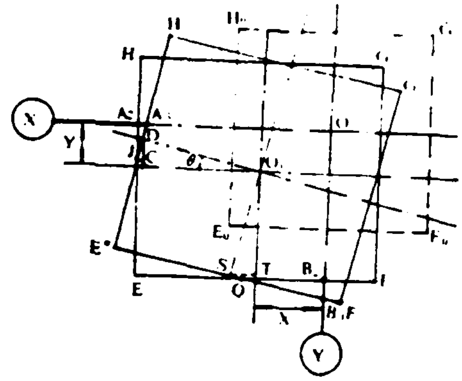

Fig. 4 Movement of Contact Point on Measuring Contact Head
Fig. 5 Diagram of Rotation of Horizontal Test Measuring Surface $\theta<0$

Going through a practical derivation clearly shows that the six situations all possess the same type of expression. In this case, it is only necessary to do calculations for one situation.

$$0^\circ \leqslant \psi_z < 45^\circ, \alpha > 0, \beta < 0, \theta < 0, X > 0, Y > 0$$

θ is the angle of rotation around the OZ coordinate axis. It is obvious that the horizontal test measurement surface rotates through angle θ in the same way. Analysis of the front surface down to the mutual influences of the angles of deflection α and β cause the horizontal test measurement surface to give rise to deformation. After making adjustments, α and β are used independently to cause the horizontal test measurement surface to give rise to deformations in $\square E''F''G''H''$ as in the diagram, and rotate it through the angle θ ; that is, becoming $\square E'''F'''G'''H'''$, as shown in Fig. 5.

From Fig. 5 one can see that the angle θ causes the X sensor and Y sensor to respectively acquire an additional amount of displacement becoming $A_1''A_3$ and $B_1''B_3$.

Solving for $A_1''A_3$, the D point coordinates are

$$\begin{cases} X_D = X + O_1 D\cos\theta \\ Y_D = Y - O_1 D\sin\theta \end{cases}$$

$\because\ A_1O_1 = O_1D_1$, 又 $A_1'O = X' = X + (R+R_0)\left(\frac{1}{\cos\alpha} - 1\right) = X + A_1O_1$

(63

$\therefore O_1D = A_1O_1 = (R+R_0)\left(\frac{1}{\cos\alpha} - 1\right)$, also because $DC = O_1D\sin\theta < 0$, therefore, the D point coordinate should be:

$$\begin{cases} X_D = X + (R+R_0)\left(\frac{1}{\cos\alpha} - 1\right)\cos\theta \\ Y_D = Y + (R+R_0)\left(\frac{1}{\cos\alpha} - 1\right)\sin\theta \end{cases} \qquad (12)$$

Make $H'''E'''$ and $H''E''$ cross at point J. Then, the equation for the straight line DJ is:

$$Y = -\frac{1}{tg\,\theta}(X - X_D) + Y_D \qquad (13)$$

Also one has:

$$X_J = X' = X + (R+R_0)\left(\frac{1}{\cos\alpha} - 1\right) \qquad (14)$$

Take equation (14) and substitute in equation (13):

$$y_J = -\frac{1}{tg\,\theta}\left[(R+R_0)\left(\frac{1}{\cos\alpha} - 1\right)(1-\cos\theta)\right] + Y + (R+R_0)\left(\frac{1}{\cos\alpha} - 1\right)\sin\theta \qquad (15)$$

From $Rt\Delta A_1''A_3J$ we get: $A_1''A_3 = Y_J tg\,\theta$

$$\therefore A_1''A_3 = (R+R_0)\left(\frac{1}{\cos\alpha} - 1\right)\left(\frac{1}{\cos\theta} - 1\right) + Y tg\,\theta \qquad (16)$$

From Fig. 5 we get the geometrical relationship

$$A_3O + A_3''A_3 = A_3''O = X'$$

$$A_3O = X'', A_3''A_3 = y, \mathrm{tg}\,\theta < 0 \quad \therefore A_3O - A_3''A_3 - A_3''A_3 = A_3O$$

Substituting the various algebraic quantities and simplifying, we get:

$$X = X'' - Y(\mathrm{tg}\,r + \mathrm{tg}\,\theta) - (R+R_0)\left(\frac{1}{\cos\alpha} - 1\right)\frac{1}{\cos\theta} - R_0\cos\alpha\left(\frac{1}{\cos r} - 1\right) \tag{17}$$

In solving for $B_3''B_3$, we use a process identical to that used in solving for $A_3''A_3$, and we obtain an S point coordinate which is:

$$\begin{cases} X_S = X - (R+R_0)\left(\frac{1}{\cos\beta} - 1\right)\sin\theta \\ Y_S = Y + (R+R_0)\left(\frac{1}{\cos\beta} - 1\right)\cos\theta \end{cases} \tag{18}$$

Let $E'''F'''$ and $E''F''$ cross at point Q. The straight line equation of SQ is

$$Y = \mathrm{tg}\,\theta(X - X_S) + Y_s \tag{19}$$

The Q point coordinate is: (20)

$$Y_Q = Y' = Y + (R+R_0)\left(\frac{1}{\cos\beta} - 1\right)$$

Take equations (20)(18) and substitute in equation (19):

$$X_Q = \frac{1}{\mathrm{tg}\,\theta}(R+R_0)\left(\frac{1}{\cos\beta} - 1\right)(1 - \cos\theta) + X - (R+R_0)\left(\frac{1}{\cos\beta} - 1\right)\sin\theta \tag{21}$$

From $Rt\Delta B_3B_3''Q$ it is possible to obtain $B_3''B_3 = X_Q\,\mathrm{tg}\,\theta$

Or
$$B_3''B_3 = (R+R_0)\left(\frac{1}{\cos\beta} - 1\right)\left(1 - \frac{1}{\cos\theta}\right) + X\,\mathrm{tg}\,\theta \tag{22}$$

The geometrical relationship has the form: $B_3O - B_3''B_3 = B_3''O$

$\because B_1''B_1 = X_0 \operatorname{tg}\theta < 0$; at the same time, after giving consideration to the superposition quantities for $B_1''B_1$, one then has:

$$Y = Y'' - X(\operatorname{tg} r - \operatorname{tg}\theta) - (R+R_0)\left(\frac{1}{\cos\beta} - 1\right)\frac{1}{\cos\theta} - R_0\cos\beta\left(\frac{1}{\cos r} - 1\right) \tag{23}$$

Equations (17) and (23) are the equations for calculating the amount of displacement adjustment which is measured by the displacement sensors in the X and Y directions during omni-axial oscillation. The two are both functions, and, set up together, they can be solved for an equation through which the amount of displacement (X, Y) can be calculated from the measured amount (X'', Y'') :

$$X_{ji} = \frac{X_{ji}'' - Y_{ji}''(\operatorname{tg} r_i + \operatorname{tg}\theta_i) - (R+R_0)\frac{1}{\cos\theta_i}\left[\left(\frac{1}{\cos\alpha_i} - 1\right) - \left(\frac{1}{\cos\beta_i} - 1\right)\cdot(\operatorname{tg} r_i + \operatorname{tg}\theta_i)\right] - R_0\left(\frac{1}{\cos r_i} - 1\right)[\cos\alpha_i - \cos\beta_i(\operatorname{tg} r_i + \operatorname{tg}\theta_i)]}{1 - \operatorname{tg}^2 r_i + \operatorname{tg}^2\theta_i} \tag{24}$$

$$Y_{ji} = \frac{Y_{ji}'' - X_{ji}''(\operatorname{tg} r_i - \operatorname{tg}\theta_i) - (R+R_0)\frac{1}{\cos\theta_i}\left[\left(\frac{1}{\cos\beta_i} - 1\right) - \left(\frac{1}{\cos\alpha_i} - 1\right)\cdot(\operatorname{tg} r_i - \operatorname{tg}\theta_i)\right] - R_0\left(\frac{1}{\cos r_i} - 1\right)[\cos\beta_i - \cos\alpha_i(\operatorname{tg} r_i - \operatorname{tg}\theta_i)]}{1 - \operatorname{tg}^2 r_i + \operatorname{tg}^2\theta_i} \tag{25}$$

In the equations $j = 1, 2, i = 0, 1 \cdots\cdots n$

R, R_0 —— constants; $\alpha_i, \beta_i, r_i, \theta_i$ are calculated from the formulas given below.

(3) Calculation of Angle of Oscillation

From the definitions of the various angles of rotation one can have:

$$\operatorname{tg}\alpha_i = \frac{X_{2i} - X_{1i}}{Z_2 - Z_1} = \frac{X_{2i}'' - X_{1i}'' - (Y_{2i}'' - Y_{1i}'')(\operatorname{tg}\alpha_i \operatorname{tg}\beta_i + \operatorname{tg}\theta_i)}{(1 - \operatorname{tg}^2\alpha_i \operatorname{tg}^2\beta_i + \operatorname{tg}^2\theta_i)Z_0} \tag{26}$$

$$\operatorname{tg}\beta_i = -\frac{Y_{2i} - Y_{1i}}{Z_2 - Z_1} = \frac{Y_{1i}'' - Y_{2i}'' + (X_{2i}'' - X_{1i}'')(\operatorname{tg}\alpha_i \operatorname{tg}\beta_i - \operatorname{tg}\theta_i)}{(1 - \operatorname{tg}^2\alpha_i \operatorname{tg}^2\beta_i + \operatorname{tg}^2\theta_i)Z_0} \tag{27}$$

Calculation of the Angle θ_i : From equation (17) it is possible to obtain:

$$X_{2i}=X''_{2i}-Y_{2i}(\mathrm{tg}\, r_i+\mathrm{tg}\,\theta_i)-(R+R_0)\left(\frac{1}{\cos\alpha_i}-1\right)\frac{1}{\cos\theta_i}-R_0\cos\alpha_i\left(\frac{1}{\cos r_i}-1\right)$$

Through deduction it is possible to obtain:

$$X_{3i}=X''_{3i}-(Y_{2i}+Y_0)(\mathrm{tg}\, r_i+\mathrm{tg}\,\theta_i)-(R+R_0)\left(\frac{1}{\cos\alpha_i}-1\right)\frac{1}{\cos\theta_i}$$

$$-R_0\cos\alpha_i\left(\frac{1}{\cos r_i}-1\right) \tag{28}$$

From the definition:

$$\mathrm{tg}\,\theta_i=\frac{X_{3i}-X_{2i}}{Y_0}=\frac{X''_{3i}-X''_{2i}}{2Y_0}-\frac{1}{2}\mathrm{tg}\, r_i \tag{29}$$

Equations (26)(27)(29) are a set of implicit transcendental equations. Using the iterative substitution method in a computer application, one solves for values of $\alpha_i, \beta_i, \theta_i$. After this, one then substitutes equations (24) and (25). It is then possible to solve for X_{1i} and Y_{1i} for the various amounts of displacement.

(4) Adjustment of the Numerical Data Measured By the Displacement Sensor Z_3

Definition: The angle of oscillation is the angle included between the geometrical center line of the jet tube and the OZ coordinate axis. It is expressed by the use of ϑ . (65

The numerical data recorded by the Z_3 sensor, alone, due to the angle of slant on the Z plate, introduces an additional amount of displacement. Moreover, this angle of slant is always equal to oscillation angle ϑ . In order to solve for this oscillation angle, one must first solve for the direction number of the geometrical center line

$$A_i=X_{2i}-X_{1i};B_i=Y_{2i}-Y_{1i};C=Z_2-Z_1=Z_0 \tag{30}$$

Oscillation angle ϑ : $$\cos\vartheta_i = \frac{C}{\sqrt{A_i^2 + B_i^2 + C^2}} \qquad (31)$$

Adjustment calculation for Z_{3i}'' : $$Z_{3i} = Z_{3i}'' - R_i\left(\frac{1}{\cos\vartheta_i} - 1\right) \qquad (32)$$

In a heat test bed situation, it is possible to make use of two displacement sensors Z_{3A} and Z_{3B} in order to replace sensor Z_3 . Z_{3A} and Z_{3B} are installed symmetrically on the two sides of the jet tube in order to avoid ignition flame heat corrosion.

As Fig. 6 shows

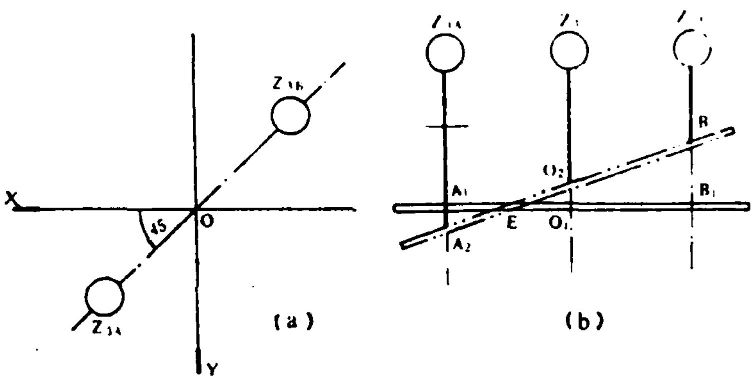

Fig. 6 (a) Chart of Sensor Distribution (b) A Comparison of Sensors Z_{3A} and Z_{3B} to Sensor Z_3

It is easy to demonstrate that, between Z_{3A} , Z_{3B} and Z_3, there is the relationship shown below:

$$Z_3'' = (Z_{3A}'' + Z_{3B}'')/2 \qquad (33)$$

(5) Adjustment of the Coordinates of Actuator Tube Fixing Points to Control the Direction and Amount of Thrust

Due to the results of pressure contents and the forces used with actuator tubes, the displacement of the rod fixing point along the axis reaches above 5mm. This not only produces an influence on the shock process of the actuator tubes. It is also related to the direction of the forces used and the force momentum. Therefore, it is necessary to make adjustments to the measured amounts. Most of the amount of the change is along the direction of the axis. Therefore, the adjustment is approximately:

$$\begin{cases} Z_{01i}=H_0+H''_{1i} \\ Z_{02i}=H_0+H''_{2i} \end{cases} \tag{34}$$

In the equations, H_0 is the coordinate of the rod fixing point. H''_{1i}, H''_{2i} are the values of the amounts measured.

(6) Calculations of the Motive Forces F_{1i} and F_{2i} Used to Control the Amount and Direction of Thrust P,

As motive force one can choose to use the tensile pressure sensor contact measurements obtained as F_{1i} and F_{2i} . Or, one can measure the pressure differential P on the two sides of the piston. The force used is then:

$$F_{ji}=SP_{ji}$$

In the equation, S is the area of the piston, $j=1,2, i=1,2,\cdots n$.
Up to the present time, we have solved for the following parameters:

$$X_{3i}, X_{2i}, X_{1i}, Y_{2i}, Y_{1i}, Z_{3i}, Z_{01i}, Z_{02i}, F_{1i}, F_{2i}, a_i, \beta_i, \theta_i, r_i, \delta_i, A_i, B_i$$

and C , as well as constants to be used in later calculations. It is not necessary to explain these for our purposes here. (66

2, Calculation of Center of Oscillation for Flexible Jet Tube

THE CONCEPT OF A CENTER OF OSCILLATION

As far as the concept of a center of oscillation for flexible jet tubes is concerned, both inside and outside China, there have been treatments in a number of technical reports. But, these reports have not found a clear and precise definition. Moreover, there have been several methods put forward which are obscure and unclear. Before making calculations of the center of oscillation, we plan to have a clear and precise concept to act as a theoretical guide for analysis and calculations.

What is called a center of oscillation must be understood in the following terms. In the case of rigid bodies, there are, of course plane oscillations taking place as well as spatial oscillations (omni-axial oscillation). Both of these exist simply as a series of instantaneous axial rotations, and no instantaneous center of oscillation exists. Obviously, a jet tube is a rigid body, and its center of oscillation can change.

Flexible jet tubes also have a point which functions as their theoretical center of oscillation. If the design and manufacture of the flexible connector heads are both absolutely ideal, this leads to the flexible jet tube rotating around the same fixed point. What are called its instantaneous axes of rotation all pass through its theoretical center of oscillation.

Absolute idealization of flexible jet tubes does not exist. In reality, due to content pressure (or combustion chamber pressure) changes, flexible jet tubes are made to produce relatively large amounts of axial instability. Besides this, flexible connector heads do not have uniform distribution of material around their circumference, and, during oscillation, their acceptance of forces will not be entirely symmetrical. It is also impossible that the deformations in the flexible connector heads, which are caused by this, should be symmetrical and uniform. This will also cause the instantaneous axis of rotation of flexible jet tubes not to pass through their theoretical center of oscillation. When flexible jet tubes undergo omni-axial oscillation under various types of content pressures, the series of instantaneous axes of rotation will form a cylinder-shaped included figure. This figure will be symmetrical around the center of oscillation which will be included in it. This is called the "oscillation center" for short. This is also nothing else except the actual oscillation center of the jet tube, the size of the geometrical dimensions of which reflect the qual ity characteristics and rigidity of the flexible connector heads.

If one is considering directly solving for the geometrical range of the included center of oscillation, it is necessary to have dense instantaneous axes of rotation. It is also necessary to have large amounts of experimental data. It is difficult to get to this point, and it is also not economical. On the basis of this special characteristic of jet tubes rotating around these fixed points, it is possible to reach the conclusion which follows. The instantaneous oscillation center of the geometrical center line of jet tubes, is always a reduplication of this fixed point. This fixed point is what is called the oscillation center of the jet tube. Because of this, we then use the instantaneous oscillation center of the geometrical center line of a jet tube to replace the point center of oscillation of the jet tube. By means of this method, we use a limited amount of experimental data to solve for the geometrical size range of the jet tube oscillation center. Moreover, this supplies a reference point for solving for the instantaneous moment of force of oscillation.

During oscillation, if the geometrical center lines cross each other, the results of the calculations discussed above are completely accurate. However, it is also possible for them to be mutually off and not cross. In such a case, one then takes their "average oscillation plane" and solves for the oscillation center. Obviously, the results of this are approximate. The degree of this approximation varies with and increases as the degree of graduation of the measured angle of oscillation is reduced. Experimentation clearly shows that, when the measured angle of oscillation is changed from 15 degrees to 1.5 degrees, the distance between two adjacent geometrical center lines drops from 0.5mm to 0.2mm, roughly speaking.

CALCULATION OF THE OSCILLATION CENTER OF FLEXIBLE JET TUBES

In order to simplify the discussion, let the geometrical center line of the jet tube be the Z' axis. This is not the same as the axis of the coordinate system.

The Z' axis equation is:

$$\frac{X-X_{1i}}{A_i}=\frac{Y-Y_{1i}}{B_i}=\frac{Z-Z_1}{C} \quad (35)$$

The equation for the Z plate plane is

$$A_iX+B_iY+C(Z-Z_{1i})=0 \quad (36)$$

The set of simultaneous equations (35) (36) gives us the coordinates for the O_i point. The O_i point coordinates are:

$$z_{0_i}=\frac{CZ_{1i}-A_iQ_i-B_iP_i}{A_iK_i+B_il_i+C} \quad (37)$$

$$x_{0_i}=K_iz_{0_i}+Q_i$$

$$y_{0_i}=l_iz_{0_i}+P_i$$

In the equations $K_i = A_i / C ; Q_i = X_{1i} - K_{1i} Z_1 ; L_i = B_i / C ; P_i = Y_{1i} - l_i Z_1$

The O_i point is a point on the Z' axis. In the initial configuration, it is a duplication of the origin point of the coordinate system.

If we postulate two mutually adjacent instants, the plane at O_i which contains the instantaneous center of oscillation is π_{1i}. We then have:

$$(x-x_{0i})^2+(y-y_{0i})^2+(z-z_{0i})^2=(x-x_{0i-1})^2+(y-y_{0i-1})^2+(z-z_{0i-1})^2$$

After rearrangement, we get: $\pi_{1i}: \; A_{1i}x+B_{1i}y+C_{1i}z=D_{1i}$ (38)

In the equations

$$\begin{cases} A_{1i}=x_{0i}-x_{0i-1} ; B_{1i}=y_{0i}-y_{0i-1} ; C_{1i}=z_{0i}-z_{0i-1} \\ D_{1i}=(x_{0i}^2+y_{0i}^2+z_{0i}^2-x_{0i-1}^2-y_{0i-1}^2-z_{0i-1}^2)/2 \end{cases}$$

In order to solve for the instantaneous axis of rotation of jet tubes, one must still find a second point on the plane on which we find the center of oscillation for the time interval during the same period. Let this be the intersection line of the plane π_{3i}, π_{3i} and the plane π_{1i}, and one then has the instantaneous axis of rotation. Because of the fact that a measurement error in the system is unavoidable, it is only when $\pi_{3i} \perp \pi_{1i}$ that the degree of precision associated with the axis of rotation which we find is optimum. The O_i point is a fixed point on the jet tube axis line. Points which satisfy the condition $\pi_{3i} \perp \pi_{1i}$ will vary with changes in the oscillation of the jet tube. The method for the fixing of coefficients is none other than an unceasing pursuit of these points.

If we take the plane π_{4i}, and set $\pi_{4i} \parallel \pi_{1i}$

$$\pi_{4i}: \quad A_{1i}x+B_{1i}y+C_{1i}z=D_{xi} \tag{39}$$

If we solve the simultaneous equations (35) and (39).

Let the intersection point of π_{4i} and the Z_{i-1} axis be $E_{4i}(x_{4i}, y_{4i}, z_{4i})$. When we solve, we get the result:

The coordinates for point E_{3i} :

$$z_{3i}=\frac{(D_{3i}-A_{1i}Q_{i-1}-B_{1i}P_{i-1})}{A_{1i}K_{i-1}+B_{1i}L_{i-1}+C_{1i}}=K_{3i}D_{3i}+Q_{3i} \tag{40}$$

$$x_{3i}=K_{1i}D_{3}+Q_{1i}$$

$$y_{3i}=K_{2i}D_{3}+Q_{2i}$$

In the equations

$$K_{3i}=1/(A_{1i}K_{i-1}+B_{1i}L_{i-1}+C_{1i})$$

$$Q_{3i}=-(A_{1i}Q_{i-1}+B_{1i}P_{i-1})/(A_{1i}K_{i-1}+B_{1i}l_{i-1}+C_{1i})$$

$$K_{1i}=K_{i-1}K_{3i} \qquad K_{2i}=L_{i-1}K_{3i}$$

$$Q_{1i}=K_{i-1}Q_{3i}+Q_{i-1} \qquad Q_{2i}=L_{i-1}Q_{3i}+P_{i-1}$$

Make the intersection point of plane π_{3i} and axis Z_i' be $E_{3i}(x_{3i},y_{3i},z_{3i})$. When we solve, we get the result:

Coordinates for point E_{3i}

$$\begin{cases} z_{3i}=\dfrac{D_{3i}-A_{1i}Q_{i}-B_{1i}P_{i}}{A_{1i}K_{i}+B_{1i}L_{i}+C_{1i}}=L_{3i}D_{3i}+P_{3i} \\ x_{3i}=L_{1i}D_{3i}+P_{1i} \\ y_{3i}=L_{2i}D_{3i}+P_{2i} \end{cases} \tag{41}$$

in the equations:

$$L_{3i}=\frac{1}{A_{1i}K_{i}+B_{1i}L_{i}+C_{1i}}, \qquad P_{3i}=\frac{-(A_{1i}Q_{i}+B_{1i}P_{i})}{A_{1i}K_{i}+B_{1i}L_{i}+C_{1i}}$$

$$L_{1i}=K_{i}L_{3i} \qquad P_{1i}=Q_{i}+K_{i}P_{3i}$$

$$L_{2i}=L_{i}L_{3i} \qquad P_{2i}=P_{i}+L_{i}P_{3i}$$

The meanings of the coefficients K_i, L_i, P_i, Q_i [illegible] and [illegible]

[illegible] E_{3i} [illegible] E_{3i} [illegible] In this way, [illegible] condition [illegible] $Q_{3i}E_{3i}=O_iF_{3i}$ [illegible]

$$(x_{0i-1}-x_{0i})^2+(y_{0i-1}-y_{0i})^2+(z_{0i-1}-z_{0i})^2=(x_{0i}-x_{3i})^2+(y_{0i}-y_{3i})^2+(z_{0i}-z_{3i})^2$$

(68

After one takes equations (40) and (41) and substitutes them in an expansion arrangement, one has

$$U_{0i}D_{si}^2+V_{0i}D_{si}+W_{0i}=0 \tag{42}$$

in the equations

$$U_{0i}=l_{3i}^2+l_{2i}^2+l_{1i}^2-K_{3i}^2-K_{2i}^2-K_{1i}^2$$

$$V_{0i}=2[K_{1i}(x_{0i-1}-Q_{1i})+K_{2i}(y_{0i-1}-Q_{2i})+K_{3i}(z_{0i-1}-Q_{3i})-L_{1i}(x_{0i}-P_{1i})-L_{2i}(y_{0i}-P_{2i})-L_{3i}(z_{0i}-P_{3i})]$$

$$W_{0i}=(x_{0i}-P_{1i})^2+(y_{0i}-y_{2i})^2+(z_{0i}-P_{3i})^2-(x_{0i-1}-Q_{1i})^2-(y_{0i-1}-Q_{2i})^2-(z_{0i-1}-Q_{3i})^2$$

Solving equation (42) we have:

$$D_{si1,2}=\frac{-V_{0i}\pm\sqrt{V_{0i}^2-4U_{0i}W_{0i}}}{2U_{0i}} \tag{43}$$

$D_{si1,2}$ is then the fixed coefficient we were solving for. There are two sets of solutions. However, corresponding to our actual problem, only the solution set in which z_{0i} and z_{0i} are simultaneously smaller than zero is applicable. Therefore, we take the two solution sets of which we solved for $D_{si1,2}$ and substitute them respectively into equations (40) and (41). From the principles discussed above, we decide and make a selection. Because of this, after we make a decision, the solutions of (40) and (41) which we chose, then make it possible to solve for the plane π_{3i} on which is located the simultaneous oscillation center for all different points on the jet tube. Moreover, $\pi_{3i}\perp\pi_{3i}$. Its [illegible]

$$(x-x_{0i})^2+(y-y_{0i})^2+(z-z_{0i})^2=(x-x_{0i})^2+(y-y_{0i})^2+(z-z_{0i})^2$$

$$A_{3i}x+B_{3i}y+C_{3i}y=D_{3i} \tag{44}$$

in the equations

$$\begin{cases} A_{3i}=x_{9i}-x_{8i}, B_{3i}=y_{9i}-y_{8i}, C_{3i}=z_{9i}-z_{8i} \\ D_{3i}=(x_{9i}^2+y_{9i}^2+z_{9i}^2-x_{8i}^2-y_{8i}^2-z_{8i}^2)/2 \end{cases}$$

The line of intersection between planes π_{1i} and π_{3i} is the instantaneous axis of rotation we are solving for. Below, we also solve for the plane of oscillation of the geometrical center line Z' axis of the jet tube, and we let this plane be π_{2i} .

During omni-axial oscillation of flexible jet tubes, the most general situation for the track of the Z' axis is a curved surface in space. If we take this curved surface and divide it into n partial curved surfaces, and, respectively use a plane to approximately replace their various oscillation planes π_{2i} , it is obvious that, when the dissected areas n are increased in number, the level of the approximation is raised. We select the number n so as to satisfy the requirement for precision which happens to exist. In order to solve for the oscillation plane π_{2i} , one first does the calculations set out below:

(i) The direction number N_i of the common perpendicular line between the jet tube axis line Z'_{i-1} and Z'_i for two adjacent instants.

Make the direction numbers of the axis lines Z'_{i-1} and Z'_i respectively N_{1i} and N_{2i} , then:

$$N_i=\{A_{i-1},B_{i-1},C\}\times\{A_i,B_i,C\}=\{A_{2i},B_{2i},C_{2i}\} \tag{45}$$

in the equations

$$A_{2i}=C(B_{i-1}-B_i); B_{2i}=C(A_i-A_{i-1}); C_{2i}=A_{i-1}B_i-A_iB_{i-1}$$

(ii) Make plane R_{i-1}, contain axis Z'_{i-1} . And, make it parallel to N_i. Then, the equation for R_{i-1} is

$$R_{i-1}: \begin{vmatrix} x-X_{1i-1}, & y-Y_{1i-1}, & z-Z_1 \\ A_{i-1}, & B_{i-1}, & C \\ A_{2i}, & B_{2i}, & C_{2i} \end{vmatrix}=0$$

Or it is: $$A_{8i}x+B_{8i}y+C_{8i}z=D_{8i} \tag{46}$$

in the equations

$$A_{8i}=B_{i-1}C_{2i}-B_{2i}C,\ B_{8i}=A_{2i}C-A_{i-1}C_{2i}$$
$$C_{8i}=A_{i-1}B_{2i}-A_{2i}B_{i-1},\ D_{8i}=A_{8i}X_{1i-1}+B_{8i}Y_{1i-1}+C_{8i}Z_1$$

(iii) Make the plane R_i, contain the axis Z', and make it parallel to N_i, Then, the equation for R_i is: (69

$$R_{i}: \begin{vmatrix} x-X_{1i}, y-Y_{1i}, z-Z_1 & & \\ A_i, & B_i, & C \\ A_{2i}, & B_{2i}, & C_{2i} \end{vmatrix} = 0$$

Or $$A_{8i}x+B_{8i}y+C_{8i}z=D_{8i} \tag{47}$$

in the equations

$$A_{8i}=B_iC_{2i}-B_{2i}C \qquad B_{8i}=A_{2i}C-A_iC_{2i}$$
$$C_{8i}=A_iB_{2i}-A_{2i}B_i, \qquad D_{8i}=A_{8i}X_{1i}+B_{8i}Y_{1i}+C_{8i}Z_1$$

The intersection line between the planes R_{i-1} and R_i are the mutually perpendicular lines Z'_{i-1} and the Z'_i axis because of the fact that the direction number n_i of the line of intersection is equal to the vector area $(N_{1i}\times N_{2i})$ of the direction number of Z'_{i-1} and the Z'_i axis.

The various simultaneous equations (35),(46),(47) necessarily make it possible to solve for the intersection point of the mutually perpendicular lines of the Z'_{i-1} and Z'_i axes . The reason for this is that the intersection line of R_i and R_{i-1}. is located on R_{i-1} on the one hand, and, therefore, crosses the Z'_{i-1} axis, but, on the other hand is also located on the plane R_i , and, therefore, must necessarily also cross Z'_i , as is shown in Fig. 7.

(iv) In solving for the intersection point E_{i-1} of the mutually perpendicular lines and the Z'_{i-1} axis, take the equation for the axis line Z'_{i-1} and change it to be of the form of a parametric equation.

From equation (35) we get:

$$\begin{cases} x=A_{i-1}t+X_{1i-1} \\ y=B_{i-1}t+Y_{1i-1} \\ z=Ct+Z_1 \end{cases} \tag{48}$$

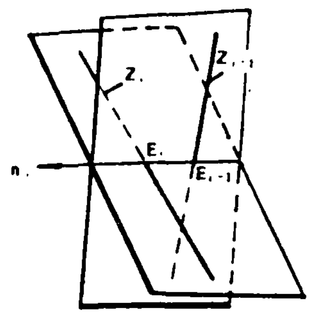

Fig. 7 The Mutually Perpendicular Lines of the Geometrical Center Lines for Two Adjacent Instants During Jet Tube Oscillation

If we take equation (48) and substitute in equation (47), and, we also make $t = K_{ei}$, we then have:

$$K_{ei} = (D_{ei} - A_{ei}X_{1i-1} - B_{ei}Y_{1i-1} - C_{ei}Z_1)/(A_{ei}A_{i-1} + B_{ei}B_{i-1} + C_{ei}C) \qquad (49)$$

If we take K_{ei} and make iterative substitutions into equation (48), we then obtain coordinates for the intersection point E_{i-1} of the mutually perpendicular lines:

$$E_{i-1i}\begin{cases} x_{Ei-1} = A_{i-1}K_{ei} + X_{1i-1} \\ y_{Ei-1} = B_{i-1}K_{ei} + Y_{1i-1} \\ z_{Ei-1} = CK_{ei} + Z_1 \end{cases} \qquad (50)$$

(v) In solving for the intersection point E_i of the mutually perpendicular lines with the Z_i axis:

Change the straight line equation of the axis Z_i to a parametric form:

$$\begin{cases} x = A_i t + X_{1i} \\ y = B_i t + Y_{1i} \\ z = Ct + Z_1 \end{cases} \qquad (51)$$

If we take equation (51) and substitute in equation (46), and we then make $t=K_{0i}$, we have:

$$K_{0i}=\frac{D_{0i}-A_{0i}X_{1i}-B_{0i}Y_{1i}-C_{0i}Z}{A_{0i}A_i+B_{0i}B_i+C_{0i}C} \tag{52}$$

If we take $K_{0i}=t$ and make iterative substitutions into equation (51), we get coordinates for the intersection point E_i of the mutually perpendicular lines and the axis Z_i' :

$$E_{ii}\begin{cases} x_{Ei}=A_iK_{0i}+X_{1i} \\ y_{Ei}=B_iK_{0i}+Y_{1i} \\ z_{Ei}=CK_{0i}+Z_i \end{cases} \tag{53}$$

It is easy to see that the points E_{i-1} and E_i are certainly not the same geometrical points on the axis line of the jet tube.

(vi) Coordinates for the center point E_{0i} of the mutually perpendicular lines $E_{i-1}E_i$ (70

Coordinates for the point E_{0i}

$$\begin{cases} x_{E0i}=(x_{Ei-1}+x_{Ei})/2 \\ y_{E0i}=(y_{Ei-1}+y_{Ei})/2 \\ z_{E0i}=(z_{Ei-1}+z_{Ei})/2 \end{cases} \tag{54}$$

From equations (45) and (54), it is possible to obtain the plane of oscillation π_{2i} from instant t_{i-1} to instant t_i of the geometrical center lines of the jet tube. That is,

$$A_{2i}(x-x_{E0i})+B_{2i}(y-y_{E0i})+C_{2i}(z-z_{E0i})=0$$

or $$A_{2i}x+B_{2i}y+C_{2i}z=D_{2i} \tag{55}$$

in the equations A_{2i}, B_{2i}, C_{2i} are the same as before.

$$D_{2i}=A_{2i}x_{E0i}+B_{2i}y_{E0i}+C_{2i}z_{E0i}$$

The system of simultaneous equations (33),(44),(55)

$$\begin{cases} A_{1i}x+B_{1i}y+C_{1i}z=D_{1i} \\ A_{2i}x+B_{2i}y+C_{2i}z=D_{2i} \\ A_{3i}x+B_{3i}y+C_{3i}z=D_{3i} \end{cases}$$

makes it possible to solve for the instantaneous center of oscillation of the geometrical center of a jet tube $C_i(x_{ci}, y_{ci}, z_{ci})$. This is also none other than a point on the center of oscillation of the jet tube. It is possible for this set of equations to be solved through the use of a computer. Therefore, we recognize that x_{ci}, y_{ci}, z_{ci} are already known. Later, we will make direct use of them. Fig. 8 is an illustrative diagram of the instantaneous axis of rotation of the jet tube and the instantaneous oscillation center of its geometrical center line.

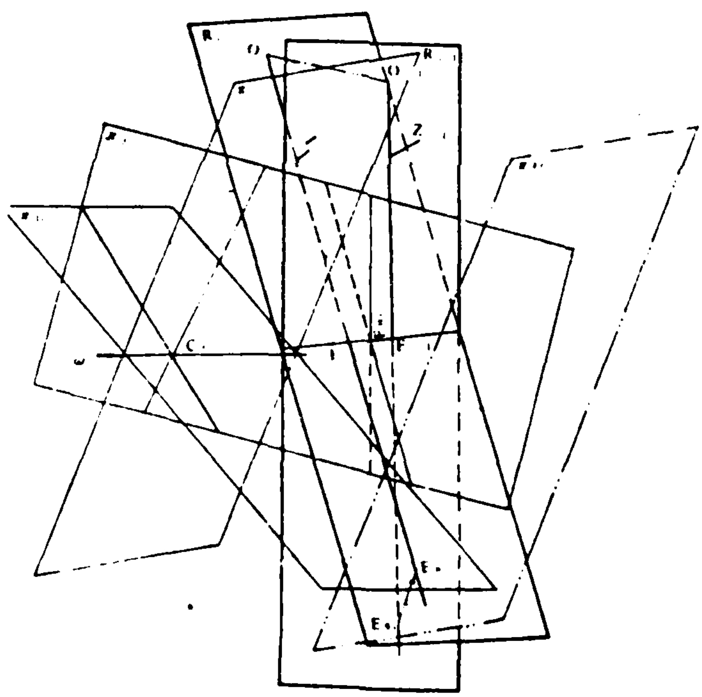

Fig. 8 Jet Tube Instantaneous Axis of Rotation and the Instantaneous Oscillation Center of Its Geometrical Center Line (1) The Line of Intersection ω_i of π_{1i} and π_{3i} is the Instantaneous Axis of Rotation of the Jet Tube (2) The Intersection Point of $\pi_{1i}, \pi_{2i}, \pi_{3i}$ is the Oscillation Center of the Z' Axis

3, Calculations of Moments of Force

The systems of moments of force which we are solving for here point, under differing designated wave forms, to a selected series of instants (or, one might say, angles of oscillation) to figure out the overall instantaneous moment of force. The focus of this article is on solving for the moment of force-angle of oscillation function relationship ($M=f(\vartheta)$). From this, it is possible to obtain the maximum and minimum (algebraic values) overall moment of force M_{max} and M_{min}, as well as its moment of force-angle of oscillation function relationship. Besides this, it is also possible, through the designation of different wave forms (normal sine waves, sawtooth waves, and square waves) to obtain the curve of the functional relationship $M=f(\vartheta)$. As far as the elaborate separating out of elastic moments of force, asymmetrical moments of force, and moments of friction, and so on, is concerned, this article makes no additional discussion. (71

After one solves for the instantaneous center of oscillation, the major contradiction in a solution for the instantaneous moment of force becomes the problems of the point of action and the direction of a system of forces in a specified space. We chose to make use of the two methods of Euler transformations and four dimensional numerical transforms, and the relative difference in values of force arms which we obtain in the solutions is not greater than 0.8%. Even so, we only introduce one method here.

(1) The Point of Action Used to Control the Direction and Amount of Thrust

From Fig. 1 one can see that the actuator tube movement points are respectively G_1 and G_2, the points of action for motive forces F_1 and F_2. Moreover, the points G_1 and G_2 are connected to the rigidity provided by the rod. Therefore, the problem becomes one of solving for the spatial coordinates of points G_1 and G_2.

(1) Selection of a dynamic coordinate system

(a) Translation coordinate system:

$GX'Y'Z'$ ---the coordinate axis which corresponds to the fixed coordinate system $QXYZ$ is always maintained parallel. The origin point G is the base on the rod center line for point G_1 (or G_2).

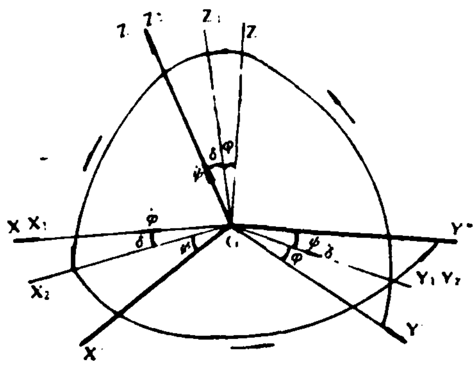

Fig. 9 The Transformation of a Dynamic Coordinate System From $GX'Y'Z' \rightarrow GX''Y''Z''$

(b) Rotary Coordinate System:

$GX''Y''Z''$ ---- the angles of rotation corresponding to the coordinate system $GX'Y'Z'$ are φ, δ, ψ, and their rotational order is as presented below: (See Fig. 9)

First, we rotate through angle φ around axis GX' , obtaining coordinate systme $GX_1Y_1Z_1$;

We also rotate through angle δ around axis GY_1 , obtaining the coordinate system $GX_2Y_2Z_2$.

Finally, we rotate through angle ψ around axis GZ_2 , obtaining coordinate system $GX''Y''Z''$. The angles φ, δ, ψ are called Euler angles.

(2) Euler Angles and Their Transformation

(a) Solving for Euler Angles

In the calculations of Part One, we already obtained the result that the angles of rotation around the various axes of the fixed coordinate system $OXYZ$ by the axis line of the jet tube are β, α, θ. . Now we must solve for the Euler angles which correspond to each instant.

From Fig. 9 it is possible to obtain the transform angular velocity projection relationship for the $GX'Y'Z'$ coordinate system.

Table 1

	$\dot{\varphi}$	$\dot{\delta}$	$\dot{\psi}$
GX'	1	0	$\sin\delta$
GY'	0	$\cos\varphi$	$-\cos\delta\cdot\sin\varphi$
GZ'	0	$\sin\varphi$	$\cos\delta\cdot\cos\varphi$

From Table 1 we get the following series of relating equations:

$$\omega_{x'}=\frac{d\beta}{dt}=\frac{d\varphi}{dt}+\sin\delta\cdot\frac{d\psi}{dt}$$
$$\omega_{y'}=\frac{d\alpha}{dt}=\cos\varphi\cdot\frac{d\delta}{dt}-\cos\delta\sin\psi\cdot\frac{d\psi}{dt}$$
$$\omega_{z'}=\frac{d\theta}{dt}=\sin\varphi\cdot\frac{d\delta}{dt}+\cos\delta\cdot\cos\varphi\cdot\frac{d\psi}{dt}$$

$$\begin{cases} d\beta=d\varphi+\sin\delta\cdot d\psi \\ d\alpha=\cos\varphi\cdot d\delta-\cos\delta\cdot\sin\varphi\cdot d\psi \\ d\theta=\sin\varphi\cdot d\delta+\cos\delta\cdot\cos\varphi\cdot d\psi \end{cases} \tag{56}$$

Coordinate transformations are only related to the results of rotational movements and do not consider the process of their rotational movements. If one desired to solve for the corresponding angles in a certain situation, it is possible to recognize that one always begins the rotational movement from zero degrees and simultaneously makes use of the method of freezing the coefficients, recognizing the use of approximately uniform rotational speed. In this way, equation (56) can be seen as becoming a set of differential equations with constant coefficients and a zero integration constant, for purposes of integration. Because of this, one has:

$$\begin{cases} \beta_i=\varphi_i+\sin\delta_i\cdot\psi_i \\ \alpha_i=\cos\varphi_i\cdot\delta_i-\cos\delta_i\sin\varphi_i\cdot\psi_i \\ \theta_i=\sin\varphi_i\delta_i+\cos\delta_i\cdot\cos\varphi_i\cdot\psi_i \end{cases} \tag{57}$$

In order to facilitate the carrying out of iterative substitution calculations, we change these to the form shown below:

$$\begin{cases} \psi_i = (\theta_i \cos\varphi_i - \alpha_i \cdot \sin\varphi_i)/\cos\delta_i \\ \varphi_i = \beta_i - \psi_i \sin\delta_i \\ \delta_i = (\alpha_i + \cos\delta_i \cdot \sin\varphi_i \cdot \psi_i)/\cos\varphi_i \end{cases} \tag{58}$$

The initial value for iterative substitution can be taken to be: $\varphi_i^0 = \beta_i, \delta_i^0 = \alpha_i/\cos\varphi_i$.

Finally, we solve for the Euler angles: $\psi_i, \varphi_i, \delta_i$.

(b) Euler Transformation

The purpose of the transformation is to carry out a solution for moments in a fixed coordinate system. On the basis of the transformation order which is given in Fig. 9, we obtain the results shown below:

Transformation of $GX''Y''Z'' \to GX_2Y_2Z_2$:

$$A_1 = \begin{pmatrix} \cos\psi, & -\sin\psi, & 0 \\ \sin\psi, & \cos\psi, & 0 \\ 0 & 0 & 1 \end{pmatrix} \tag{59}$$

Transformation of $GX_2Y_2Z_2 \to GX_1Y_1Z_1$:

$$A_2 = \begin{pmatrix} \cos\delta & 0 & \sin\delta \\ 0 & 1 & 0 \\ -\sin\delta & 0 & \cos\delta \end{pmatrix} \tag{60}$$

Transformation of $GX_1Y_1Z_1 \to GX'Y'Z'$;

$$A_3 = \begin{bmatrix} 1 & 0 & 0 \\ 0 & \cos\varphi & -\sin\psi \\ 0 & \sin\varphi & \cos\varphi \end{bmatrix} \tag{61}$$

Take the transformation matrix from $GX''Y''Z''$ to $GX'Y'Z'$ be A. Then, we have

$$A_i = \begin{bmatrix} \cos\psi_i\cos\delta_i, & -\sin\psi_i\cos\delta_i, & \sin\delta_i \\ \sin\psi_i\cos\varphi_i + \cos\psi_i\sin\delta_i \cdot \sin\varphi_i, & \cos\psi_i \cdot \cos\varphi_i - \sin\psi_i\sin\delta_i\sin\varphi_i, & -\cos\delta_i\sin\varphi_i \\ \sin\psi_i \cdot \sin\varphi_i - \cos\psi_i\sin\delta_i \cdot \cos\varphi_i, & \cos\psi_i\sin\varphi_i + \sin\psi_i \cdot \sin\delta_i\cos\varphi_i, & \cos\delta_i\cos\varphi_i \end{bmatrix} \quad (52)$$

(73

The transformation of point G_{1i} in coordinate system $GX'Y'Z'$:

$$\begin{bmatrix} x'_{G1i} \\ y'_{G1i} \\ z'_{G1i} \end{bmatrix} = A_i \begin{bmatrix} R_G \\ 0 \\ 0 \end{bmatrix} \quad (53)$$

The transformation of point G_{2i} in coordinate system $GX'Y'Z'$:

$$\begin{bmatrix} x'_{G2i} \\ y'_{G2i} \\ z'_{G2i} \end{bmatrix} = A_i \begin{bmatrix} 0 \\ R_G \\ 0 \end{bmatrix} \quad (54)$$

(3) Transformation of moving rod points G_1 and G_2 in a fixed coordinate system

As far as the translation operations of rigid bodies are concerned, the amount of displacement of each point must be equivalent. Now, in order to solve for the amount of displacement of the origin point G of the translation coordinate system:

$\because GO = H_G, \therefore$ we have $(x - x_{0i})^2 + (y - y_{0i})^2 + (z - z_{0i})^2 = H_G^2$

Solution of the simultaneous equations (35) and (65) allows us to obtain coordinates for the point G :

$$\begin{cases} z_{G_i} = (-V_i - \sqrt{V_i^2 - 4U_i W_{G_i}})/2U_i \\ x_{G_i} = K_i z_{G_i} + Q_i \\ y_{G_i} = L_i z_{G_i} + P_i \end{cases} \tag{66}$$

in the equations $U_i = K_i^2 + L_i^2 + 1; V_i = 2[K_i(Q_i - x_{0i}) + L_i(P_i - y_{0i}) - z_{0i}]$
$W_i = (Q_i - x_{0i})^2 + (P_i - y_{0i})^2 + z_{0i}^2; W_{G_i} = W_i - H_G^2$

By putting equation (63) and equation (64) together respectively with equation (66), it is possible to obtain the transformation of points G_{1i} and G_{2i} in the fixed coordinate system.

$$\begin{cases} x_{G1i} = x'_{G1i} + x_{G_i} \\ y_{G1i} = y'_{G1i} + y_{G_i} \\ z_{G1i} = z'_{G1i} + z_{G_i} \end{cases} \tag{67}$$

also

$$\begin{cases} x_{G2i} = x'_{G2i} + x_{G_i} \\ y_{G2i} = y'_{G2i} + y_{G_i} \\ z_{2i} = z'_{G2i} + z_{G_i} \end{cases} \tag{68}$$

[illegible] direction of the forces acting to control the amount and [illegible]

[illegible] direction of forces acting

[illegible] duplicate the axis line of the activator tube. [illegible] coordinates for the dynamic fulcrum and the fixed [illegible], we solve for their directional cosine.

(69)

[illegible] F_{1i} : $A_{0i} = x_{G1i} - R_0; B_{0i} = y_{G1i}; C_{0i} = z_{G1i} - H_{01i}$

[illegible] F_{2i} : $A_{0i} = x_{G2i}; B_{0i} = y_{G2i} - R_0; G_{0i} = z_{G2i} - H_{02i}$

Arm length of activator tube:

$$\left.\begin{aligned} l_{xi} &= \sqrt{A_{8i}^2 + B_{8i}^2 + C_{8i}^2} \\ l_{yi} &= \sqrt{A_{9i}^2 + B_{9i}^2 + C_{9i}^2} \end{aligned}\right\} \tag{70}$$

Directional cosine of forces acting:

$$F_{1i}\begin{cases} \cos\alpha_{1i} = A_{8i}/L_{xi} \\ \cos\beta_{1i} = B_{8i}/L_{xi} \\ \cos\gamma_{1i} = C_{8i}/L_{xi} \end{cases} \quad \text{also} \quad F_{2i}\begin{cases} \cos\alpha_{2i} = A_{9i}/L_{yi} \\ \cos\beta_{2i} = B_{9i}/L_{yi} \\ \cos\gamma_{2i} = C_{9i}/L_{yi} \end{cases} \tag{71}$$

(2) Projections of the forces acting on the various coordinate axes:

$$\begin{cases} F_{1xi} = F_{1i}\cos\alpha_{1i} \\ F_{1yi} = F_{1i}\cos\beta_{1i} \\ F_{1zi} = F_{1i}\cos\gamma_{1i} \end{cases} \quad \text{also} \quad \begin{cases} F_{2xi} = F_{2i}\cos\alpha_{2i} \\ F_{2yi} = F_{2i}\cos\beta_{2i} \\ F_{2zi} = F_{2i}\cos\gamma_{2i} \end{cases} \tag{72}$$

(3) Matrix Calculations

(1) Solve for the matrix of the instantaneous oscillation center of the geometrical center line of the jet tube

(a) Radius vector of the instantaneous oscillation center of the forces acting

$$\boldsymbol{r}_{1i} = \overline{C_i G_{1i}} \quad \text{and} \quad \boldsymbol{r}_{2i} = \overline{C_i G_{2i}} \quad \text{or}$$

$$\begin{cases} r_{1xi} = (x_{G1i} - x_{Ci})/1000 \\ r_{1yi} = (y_{G1i} - y_{Ci})/1000 \\ r_{1zi} = (z_{G1i} - z_{Ci})/1000 \end{cases} \quad \text{also} \quad \begin{cases} r_{2xi} = (x_{G2i} - x_{Ci})/1000 \\ r_{2yi} = (y_{G2i} - y_{Ci})/1000 \\ r_{2zi} = (z_{G2i} - z_{Ci})/1000 \end{cases} \tag{73}$$

(b) Overall moment of force--Main moment and its relative moments

Projections of the main moment on the various coordinate axes :

$$M_{xi} = \sum (r_{yi} F_{zi} - r_{zi} F_{yi}) = (r_{yi} F_{z} + r_{yi} F_{z} \ldots [illegible]$$

$$M_{yi} = \sum (r_{zi} F_{xi} - r_{xi} F_{zi}) = (r_{zi} F_{x} + r_{zi} F_{x} \ldots [illegible]$$

$$M_{zi} = \sum (r_{xi} F_{yi} - r_{yi} F_{xi}) = (r_{xi} F_{y} + r_{xi} F_{y} \ldots [illegible]$$

[illegible]

$$M = \sqrt{M_x^2 + M_y^2 + M_z^2}$$

[illegible]

$$M_{i} = M \ldots [illegible]$$

[illegible] F [illegible] F [illegible]

ω_i

$$\omega_i = n_i \times n_{i+1} = (A_{\omega i}, B_{\omega i}, C_{\omega i})$$

[illegible]

$$A_{\omega i} = B_i C_{i+1} - C_i B_{i+1},\ B_{\omega i} = C_i A_{i+1} - A_i C_{i+1},\ C_{\omega i} = A_i B_{i+1} - B_i A_{i+1}$$

[illegible] M_i [illegible] $\theta_{\omega i}$ [illegible]

$$\cos\theta_{\omega i} = \frac{M_{xi} A_{\omega i} + M_{yi} B_{\omega i} + M_{zi} C_{\omega i}}{\sqrt{M_{xi}^2 + M_{yi}^2 + M_{zi}^2}\,\sqrt{A_{\omega i}^2 + B_{\omega i}^2 + C_{\omega i}^2}}$$

From equations (77) and (78), we can then solve for the moment of force M [illegible] of the instantaneous axis of rotation

$$M_{\omega i} = |M_{ci}| \cos v_{\omega i} \qquad (79)$$

The corresponding specific moment of force:

$$M_{\omega ei} = |M_{\omega i}| / v_i \qquad (80)$$

[illegible] Parameters

[illegible] the Instantaneous Axis of Rotation

[illegible] ation center which we already solved [illegible] (x_{ei}, y_{ei}, z_{ei}) and $A_{\omega i}, B_{\omega i}, C_{\omega i}$, it is then possible to solve [illegible] instantaneous axis of rotation:

$$\frac{x - x_{ei}}{A_{\omega i}} = \frac{y - y_{ei}}{B_{\omega i}} = \frac{z - z_{ei}}{C_{\omega i}} \qquad (81)$$

[illegible] go through the horizontal projection diagram [illegible] axis of rotation which appears in the $X-Y$ diagram, [illegible] center of oscillation of the [illegible] equation (81), we obtain its projection equation:

$$y = K_{\omega i} x + b_i \qquad (82)$$

[illegible]:

$$K_{\omega i} = B_{\omega i} / A_{\omega i}, \quad b_i = y_{ei} - K_{\omega i} x_{ei}$$

[illegible] center line of jet tube [illegible] angle be ψ_{zi}, then:

$$\operatorname{tg} \psi_{zi} = B_i / A_i \qquad (83)$$

ψ_z [illegible] capable of changing through a range of 0-360 degrees. [illegible] the [illegible] values of A_i and B_i. Then, it is possible to precisely determine the size of ψ_{zi}.

(3) Calculation of Eccentric Thrust

Jet tubes, due to the effects of additional designated oscillations and contained pressures, are capable of causing jet tube axis lines to give rise to radial displacement, creating thrust eccentricity. This is an important technical target of flexible connector heads.

In initial configuration, the jet tube axis line equation is:

$$\frac{X-X_0}{A_0}=\frac{Y-Y_0}{B_0}=\frac{Z-Z_0}{C_0} \tag{34}$$

In the equations:

X_0, Y_0, Z_0 --- are the coordinates of a certain point on the OZ axis.

A_0, B_0, C_0 --- is the directional number of the OZ axis, which is always, for $X_0=Y_0=0, A_0=B_0=0, Z_0$ and C_0 equal to certain constants. If we let the thrust eccentricity be D_i, and we solve equations (35) and (34), we then have:

$$D_i=\frac{\left\|\begin{matrix} X_{1i}-X_0, & Y_{1i}-Y_0, & Z_i-Z_0 \\ A_0 & B_0 & C_0 \\ A_i & B_i & C_i \end{matrix}\right\|}{\sqrt{\begin{vmatrix} A_0 & B_0 \\ A_i & B_i \end{vmatrix}^2+\begin{vmatrix} B_0 & C_0 \\ B_i & C \end{vmatrix}^2+\begin{vmatrix} C_0 & A_0 \\ C & A_i \end{vmatrix}^2}}=\frac{|Y_{1i}A_i-X_{1i}B_i|}{\sqrt{B_i^2+A_i^2}} \tag{35}$$

(4) Angular Velocity of Jet Tube Oscillation

By the time function we already obtained for the angles of rotation around the various axes:

$$\beta_i=f(K\cdot\Delta T);\ a_i=f(K\cdot\Delta T);\ \theta=f(K\cdot\Delta T)\quad K=0,1,\cdots\cdots n$$

ΔT --- equidistant sampling intervals.

$$\begin{cases} \omega_{xi}=(\beta_i-\beta_{i-1})/\Delta T \\ \omega_{yi}=(a_i-a_{i-1})/\Delta T \\ \omega_{zi}=(\theta_i-\theta_{i-1})/\Delta T \end{cases} \tag{36}$$

The overall angular velocity ω_t is:

$$\omega_t = \sqrt{\omega_{xt}^2 + \omega_{yt}^2 + \omega_{zt}^2} \tag{87}$$

(5) Stroke of activator tubes

In the third section, we already solved for the instantaneous lengths of activator tubes L_{xt} and L_{yt} with the zero position length of the activator tube as L_0. From this, the stroke of the activator tubes is:

$$\begin{cases} \Delta L_{xt} = L_{xt} - L_0 \\ \Delta L_{yt} = L_{yt} - L_0 \end{cases} \tag{88}$$

(5) Spatial displacements caused by the effects of axial displacement compensation and contained jet tube pressures

This compensation is automatically carried out when the command signal is zero. After that, one carries out measurements and calculations of its spatial displacement. This is also another important technical parameter of flexible connector heads.

With jet tubes in their initial configuration (pressure zero, command zero) the electrical zero value of the mechanical apparatus and the sensors should satisfy:

$$X_{20}^{0} - X_{10}^{0} \Rightarrow 0;\ Y_{20}^{0} - Y_{10}^{0} \Rightarrow 0;\ Z_{20}^{0} = 0$$

After carrying out compensation for the effects of contained pressure, this should satisfy:

$|X_{20}' - X_{10}'| \leqslant 0.1;\ |Y_{20}^{0} - Y_{10}'| \leqslant 0.1$ We then have:

$$\begin{array}{ll} \text{Axial displacement:} & \Delta Z = Z_{20}' - Z_{20}^{0} \\ \text{Radial displacement:} & \Delta X = X_{20}' - X_{20}^{0} \\ & \Delta Y = Y_{20}' - Y_{20}^{0} \end{array} \tag{89}$$

Note: Units in all the equations and calculations are as shown below:

Length: The radii r_{II}, r_{II} use meters as a unit. All other units are mm.

Angles and angular velocities: these respectively use degrees and degrees per second as units.

Force and pressure: these respectively use kilograms and kilograms per square cm as units.

Moments of force: kilograms/meter.

Time: seconds.

REFERENCES

[1] Gagen, R. D.: Space Shuttle Solid Rocket Booster Nozzle Flexible Seal Pivot Joint Dynamics, AIAA 77-986.

[2] Solid Rocket Thrust Vector Control NASA Space Vehicle Design Criteria, NASA SP-8114, December 1974.

DISTRIBUTION LIST

DISTRIBUTION DIRECT TO RECIPIENT

ORGANIZATION	MICROFICHE
A205 DMAHTC	1
A210 DMAAC	1
B344 DIA/RTS-2C	9
C043 USAMIIA	1
C500 TRADOC	1
C509 BALLISTIC RES LAB	1
C510 R&T LABS/AVRADCOM	1
C513 ARRADCOM	1
C535 AVRADCOM/TSARCOM	1
C539 TRASANA	1
C591 FSTC	4
C619 MIA REDSTONE	1
D008 NISC	1
E053 HQ USAF/INET	1
E404 AEDC/DOF	1
E408 AFWL	1
E410 AD/IND	1
E429 SD/IND	1
P005 DOE/ISA/DDI	1
P050 CIA/OCR/ADD/SD	2
AFIT/LDE	1
FTD	
CCN	1
NIA/PHS	1
LLYL/Code L-389	1
NASA/NST-44	1
NSA/1213/TDL	2
ASD/FTD/TQIA	1

END
5-87
DTIC